



Klebsiella pneumoniae Reduces SUMOylation To Limit Host Defense Responses

Joana Sá-Pessoa,^a Kornelia Przybyszewska,^a Filipe Nuno Vasconcelos,^a Amy Dumigan,^a Christian G. Frank,^a  Laura Hobley,^a  Jose A. Bengoechea^a

^aWellcome-Wolfson Institute for Experimental Medicine, School of Medicine, Dentistry and Biomedical Sciences, Queen's University Belfast, Belfast, United Kingdom

ABSTRACT *Klebsiella pneumoniae* is an important cause of multidrug-resistant infections worldwide. Understanding the virulence mechanisms of *K. pneumoniae* is a priority and timely to design new therapeutics. Here, we demonstrate that *K. pneumoniae* limits the SUMOylation of host proteins in epithelial cells and macrophages (mouse and human) to subvert cell innate immunity. Mechanistically, in lung epithelial cells, *Klebsiella* increases the levels of the deSUMOylase SENP2 in the cytosol by affecting its K48 ubiquitylation and its subsequent degradation by the ubiquitin proteasome. This is dependent on *Klebsiella* preventing the NEDDylation of the Cullin-1 subunit of the ubiquitin ligase complex E3-SCF- β TrCP by exploiting the CSN5 deNEDDylase. *Klebsiella* induces the expression of CSN5 in an epidermal growth factor receptor (EGFR)-phosphatidylinositol 3-kinase (PI3K)-protein kinase B (AKT)-extracellular signal-regulated kinase (ERK)-glycogen synthase kinase 3 beta (GSK3 β) signaling pathway-dependent manner. In macrophages, Toll-like receptor 4 (TLR4)-TRAM-TRIF-induced type I interferon (IFN) via IFN receptor 1 (IFNAR1)-controlled signaling mediates *Klebsiella*-triggered decrease in the levels of SUMOylation via *let-7* microRNAs (miRNAs). Our results revealed the crucial role played by *Klebsiella* polysaccharides, the capsule, and the lipopolysaccharide (LPS) O-polysaccharide, to decrease the levels of SUMO-conjugated proteins in epithelial cells and macrophages. A *Klebsiella*-induced decrease in SUMOylation promotes infection by limiting the activation of inflammatory responses and increasing intracellular survival in macrophages.

IMPORTANCE *Klebsiella pneumoniae* has been singled out as an urgent threat to human health due to the increasing isolation of strains resistant to “last-line” antimicrobials, narrowing the treatment options against *Klebsiella* infections. Unfortunately, at present, we cannot identify candidate compounds in late-stage development for treatment of multidrug-resistant *Klebsiella* infections; this pathogen is exemplary of the mismatch between unmet medical needs and the current antimicrobial research and development pipeline. Furthermore, there is still limited evidence on *K. pneumoniae* pathogenesis at the molecular and cellular levels in the context of the interactions between bacterial pathogens and their hosts. In this research, we have uncovered a sophisticated strategy employed by *Klebsiella* to subvert the activation of immune defenses by controlling the modification of proteins. Our research may open opportunities to develop new therapeutics based on counteracting this *Klebsiella*-controlled immune evasion strategy.

KEYWORDS *Klebsiella pneumoniae*, SUMOylation, *let-7*, SENP2, interferon, NEDDylation

Posttranslational modifications (PTMs) are unique mechanisms that allow cells to modify rapidly and specifically the activity or interactions of proteins in a reversible process. SUMOylation is a crucial PTM involved in cell cycle, metabolism, stress response, transcription regulation, and many other biological processes. Proteomic stud-

Citation Sá-Pessoa J, Przybyszewska K, Vasconcelos FN, Dumigan A, Frank CG, Hobley L, Bengoechea JA. 2020. *Klebsiella pneumoniae* reduces SUMOylation to limit host defense responses. mBio 11:e01733-20. <https://doi.org/10.1128/mBio.01733-20>.

Editor Philippe J. Sansonetti, Pasteur Institute

Copyright © 2020 Sá-Pessoa et al. This is an open-access article distributed under the terms of the [Creative Commons Attribution 4.0 International license](https://creativecommons.org/licenses/by/4.0/).

Address correspondence to Jose A. Bengoechea, j.bengoechea@qub.ac.uk.

Received 29 June 2020

Accepted 24 August 2020

Published 29 September 2020

ies have uncovered that ~1,000 proteins are SUMO targets (1). Modification of proteins by SUMO is achieved through activation of SUMO by an E1 activating enzyme (the heterodimer SAE1/SAE2), transfer of this activated SUMO to an E2 conjugating enzyme (Ubc9), and ligation to the substrates catalyzed by different E3 ligases: members of the protein inhibitors of activated STAT (PIAS) family, RanBP2, members of the polycomb group proteins, and members of the TRIM (tripartite motif) family (2). In parallel, deconjugation of SUMO is carried by either deSUMOylating isopeptidases (DeSI enzymes DeSI-1 and DeSI-2) (3) or a family of six sentrin-specific proteases (SENPs) that cleave the inactive form of SUMO starting the SUMOylation cycle and have isopeptidase activity recycling SUMO from substrate proteins (3).

It is not surprising that pathogens target SUMOylation given its importance in controlling many pathways in eukaryotic cells. There is a wealth of evidence demonstrating that SUMOylation is involved in many aspects of cell-virus interplay, either promoting or interfering with infection (4). In contrast, the interplay between bacterial pathogens and host SUMOylation is less well understood. To date, it has been shown that the intracellular pathogens *Listeria monocytogenes*, *Shigella flexneri*, and *Salmonella enterica* serovar Typhimurium trigger an overall decrease in the SUMOylation of proteins (5–7). The three pathogens induce the degradation of the E2 enzyme Ubc9 to decrease the amount of SUMO conjugates (5–7), indicating that depletion of Ubc9 could be a preferred bacterial strategy to target SUMOylation. Recently, *S. flexneri* has also been shown to trigger the degradation of the SUMO E1 enzyme SAE2 to reduce SUMOylation (8).

We decided to study the interplay between SUMOylation and the human pathogen *Klebsiella pneumoniae*. This Gram-negative bacterium causes a wide range of infections, from urinary tract infections to pneumonia. The latter is particularly devastating among immunocompromised patients. *K. pneumoniae* is a member of the so-called ESKAPE (*Enterococcus faecium*, *Staphylococcus aureus*, *K. pneumoniae*, *Acinetobacter baumannii*, *Pseudomonas aeruginosa*, and *Enterobacter* species) group of microorganisms to emphasize that they effectively “escape” the effects of antibacterial drugs. Therefore, the development of new therapeutic strategies requires a better understanding of *K. pneumoniae* biology in the context of the complex interactions between bacterial pathogens and their hosts. This pathogen has developed sophisticated strategies to attenuate the activation of host defense (9); therefore, we hypothesized that *Klebsiella* may target SUMOylation to promote infection. A wealth of evidence underscores the importance of the Toll-like receptor (TLR)-governed inflammatory response to clear *K. pneumoniae* infections (10, 11). In turn, we and others have provided compelling evidence demonstrating that one *Klebsiella* virulence strategy is the evasion of TLR2/4-controlled antimicrobial defenses (12, 13). *Klebsiella* manipulates TLR4, epidermal growth factor receptor (EGFR), and NOD1 signaling to ablate the activation of NF- κ B and mitogen-activated protein kinases (MAPKs) (14, 15).

Here, we demonstrate that *K. pneumoniae* impairs the SUMOylation of host proteins in epithelial cells and macrophages to subvert cell innate immunity. Mechanistically, *Klebsiella* utilizes different strategies depending on the type of cell. In epithelial cells, *Klebsiella* exploits the SENP2 deSUMOylase by preventing its degradation by the ubiquitin proteasome, whereas in macrophages the decrease in SUMOylated proteins is dependent on a type I interferon (IFN)-induced microRNA (miRNA) of the *let-7* family.

RESULTS

***K. pneumoniae* decreases SUMO-conjugated proteins in epithelial cells.** To investigate whether *K. pneumoniae* affects host cell SUMOylation, we compared the global pattern of proteins conjugated to SUMO1 or SUMO2/3 in uninfected cells with that of cells infected by the wild-type hypervirulent *K. pneumoniae* strain CIP52.145 (Kp52145 here). This strain harbors the genetic determinants associated with severe human infections (16). A549 epithelial cells showed a reduction in overall SUMO1-conjugated proteins of high molecular weight (>80 kDa) after 3 h of infection, with no changes in the overall SUMO2/3-conjugated proteins (Fig. 1A). We then vali-

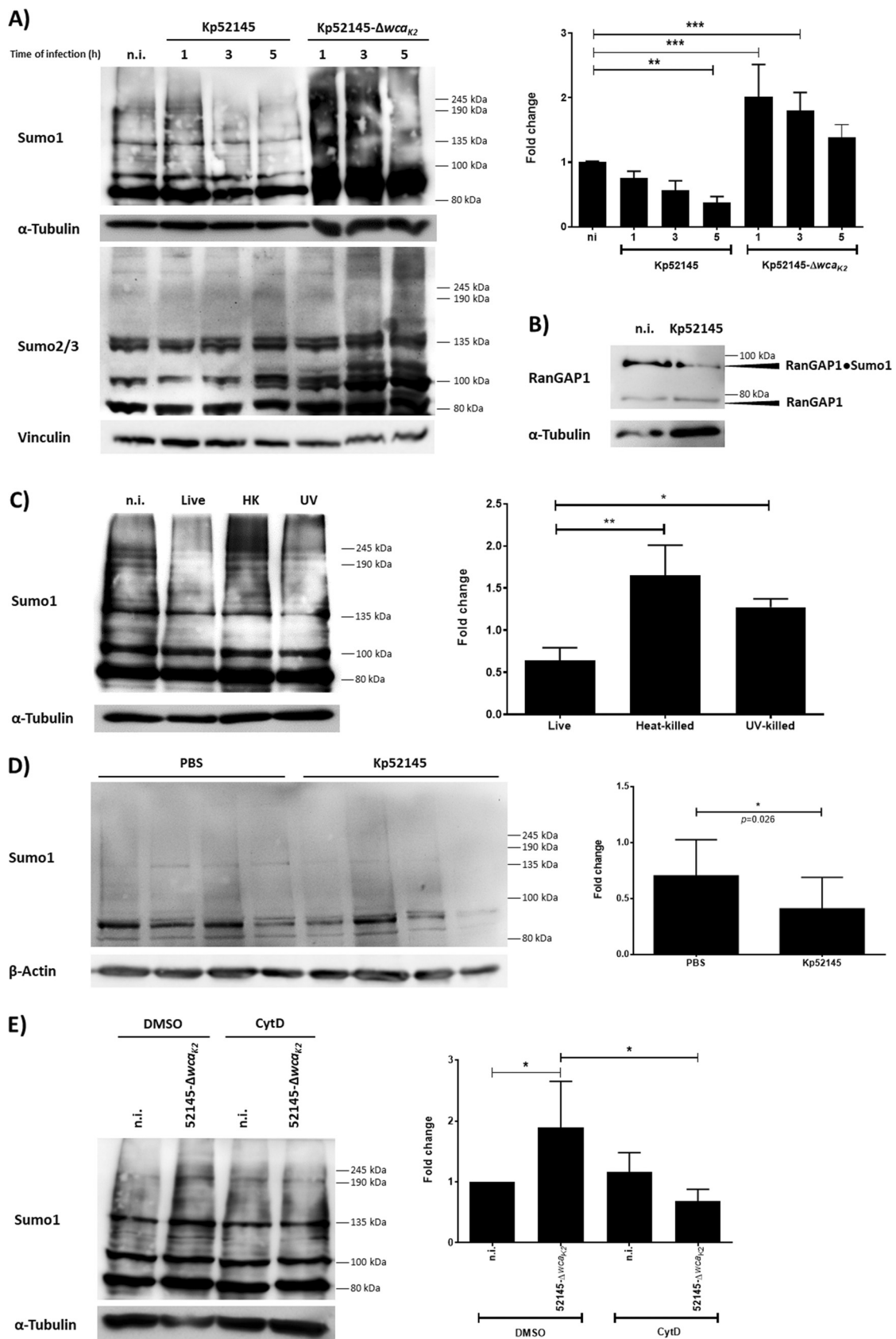


FIG 1 *K. pneumoniae* decreases SUMO-conjugated proteins in epithelial cells. (A) Immunoblot analysis of SUMO1, SUMO2/3, and tubulin levels in lysates of A549 cells infected with Kp52145 and the capsule mutant (strain 52145 Δwca_{K2}) for the indicated times. (Continued on next page)

dated the decrease in SUMOylation on the heavily SUMOylated RanGAP1 substrate. In *Klebsiella*-infected cells, we observed a clear reduction in SUMOylated RanGAP1 after 3 h postinfection (Fig. 1B). The decrease in SUMO1-conjugated proteins was also observed in NuLi-1 cells, a human primary-like airway epithelial cell line (see Fig. S1 in the supplemental material), demonstrating that the *Klebsiella*-induced decrease in overall SUMOylation was not cell type dependent. Kp52145-induced decrease in protein SUMOylation was dependent on live bacteria, because infection with either UV-killed or heat-killed bacteria caused an increase in SUMO1-conjugated proteins (Fig. 1C). To examine the relevance of these findings during infection, we assessed the pattern of SUMOylated proteins in lungs of infected mice. Although there was mouse-to-mouse variation, immunoblotting of lung homogenates revealed a decrease in the global SUMO1-conjugated proteome compared to that in homogenates from mock-infected mice (Fig. 1D). Together, our *in vitro* and *in vivo* findings reveal that *K. pneumoniae* infection leads to a decrease in the levels of SUMO-conjugated proteins.

In contrast to the wild-type strain, infection with an isogenic avirulent capsule mutant (strain 52145 Δwca_{K2}) induced an increase in SUMO1- and SUMO2/3-conjugated proteins (Fig. 1A). Since the capsule polysaccharide (CPS) abrogates the internalization of *K. pneumoniae* by A549 (17), we hypothesized that the capsule mutant-induced increase in SUMOylation is triggered by bacterial internalization. Indeed, when infections were performed in the presence of cytochalasin D, an inhibitor of *Klebsiella* internalization by epithelial cells (17), the CPS mutant did not increase the levels of SUMO1-conjugated proteins (Fig. 1E). Collectively, these results indicate that the CPS limits the increase in SUMOylation upon *Klebsiella* infection by preventing bacterial internalization.

The deSUMOylase SENP2 mediates *K. pneumoniae*-induced decrease in SUMO1-conjugated proteins in epithelial cells. We sought to gain insights into the mechanisms by which wild-type *Klebsiella* reduces the SUMOylation status in epithelial cells. Previous studies indicate that depletion of the E1 enzyme SAE2 and the E2 enzyme Ubc9 underlines bacterial pathogen-triggered decrease in SUMOylation (5–8). However, the levels of Ubc9 were not significantly affected in Kp52145-infected cells (Fig. 2A), and we did not detect any change in the levels of SAE2 or SAE1 (Fig. 2B). Although these results do not rigorously rule out that *Klebsiella* may affect the enzymatic activity of these enzymes, it prompted us to consider alternative possibilities to explain the *Klebsiella*-induced decrease in SUMOylation.

SENPs, a family of cysteine proteases, catalyze the deconjugation of SUMO from target substrates; therefore, we hypothesized that they might be involved in *Klebsiella*-triggered reduction of SUMO-conjugated proteins. SENP1 and SENP2 have nuclear localization with isopeptidase and hydrolase activity for SUMO1 and SUMO2/3 (18). SENP3 and SENP5 are localized in the nucleolus, while SENP6 and SENP7 are localized in the nucleoplasm, and all favor SUMO2/3 as the substrates (18). A small interfering RNA (siRNA)-based screen revealed an increase in the levels of SUMO1-conjugated

FIG 1 Legend (Continued)

SUMO1 smears were quantified from three independent experiments using Image Studio Lite (LI-COR) and normalized to α -tubulin. The graph represents fold change compared to noninfected control cells. n.i., not infected; **, $P \leq 0.01$; ***, $P \leq 0.001$ by one-way ANOVA with Bonferroni's multiple-comparison test. (B) Immunoblot analysis of RanGAP1 and tubulin levels in A549 infected with Kp52145 for the indicated times. (C) Immunoblot analysis of SUMO1 and tubulin levels in lysates of A549 cells infected with Kp52145 live, heat-killed for 30 min at 60°C, or UV-killed for 30 min at 10,000 J for the indicated times. SUMO1 smears were quantified from three independent experiments using Image Studio Lite (LI-COR) and normalized to α -tubulin. The graph represents fold change at 5 h of infection compared to noninfected control cells. **, $P \leq 0.01$; *, $P \leq 0.05$ by one-way ANOVA with Bonferroni's multiple-comparison test. (D) Immunoblot analysis of SUMO1 (antibody sc-9060) and tubulin levels in 50 μ g of total protein obtained from whole-lung homogenate of C57BL/6 mice infected with Kp52145 or with PBS as a mock control for 24 h. Each lane represents a lung from a different mouse. SUMO1 smears were quantified from three independent blots using Image Studio Lite (LI-COR) and normalized to β -actin. The graph represents fold change of the Kp52145 lung homogenates compared to PBS controls. Two-tailed unpaired *t* test. (E) Immunoblot analysis of SUMO1 levels in lysates of cytochalasin D- (CytD; 5 μ M, 1 h before infection) or dimethyl sulfoxide (DMSO; vehicle solution)-treated A549 cells infected with strain 52145 Δwca_{K2} for 5 h. Membranes were reprobed for tubulin as a loading control. SUMO1 smears were quantified from three independent experiments using Image Studio Lite (LI-COR) and normalized to α -tubulin. The graph represents fold change compared to DMSO noninfected control cells. *, $P \leq 0.05$ by one-way ANOVA with Bonferroni's multiple-comparison test. In all panels, data are representative of at least three independent experiments.

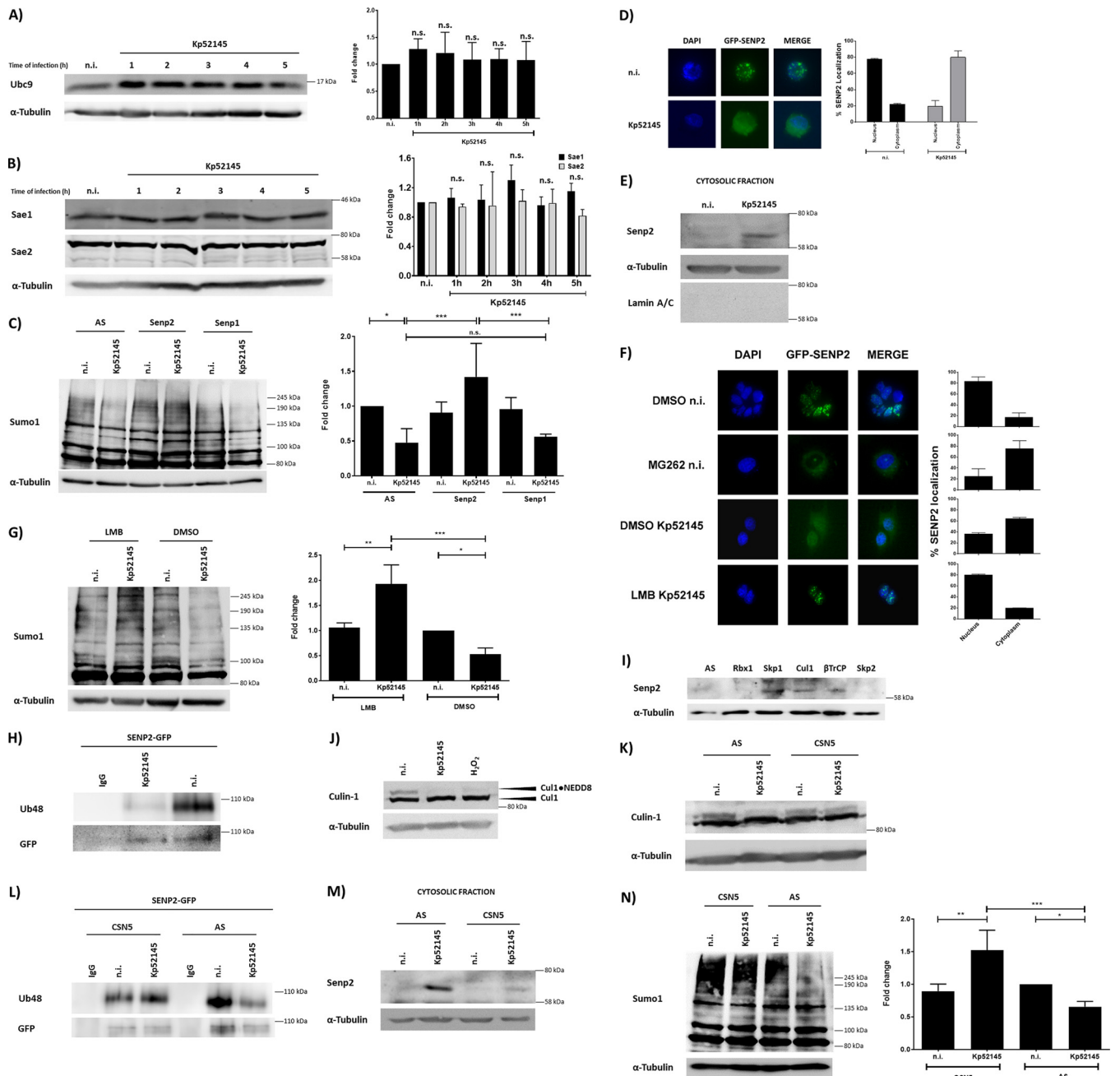


FIG 2 The deSUMOylase SENP2 mediates *K. pneumoniae*-induced decrease in SUMO-conjugated proteins. (A) Immunoblot analysis of Ubc9 and tubulin levels in lysates of A549 cells infected with Kp52145 for the indicated times. Ubc9 bands were quantified from three independent experiments using Image Studio Lite (LI-COR) and normalized to α -tubulin. The graph represents fold change compared to noninfected control cells. n.s., not significant versus n.i. determined using one-way ANOVA with Tukey's multiple-comparison test. (B) Immunoblot analysis of SAE1, SAE2, and tubulin levels in lysates of A549 cells infected with Kp52145 for the indicated times. SAE1 and SAE2 bands were quantified from three independent experiments using Image Studio Lite (LI-COR) and normalized to α -tubulin. The graph represents fold change compared to noninfected control cells. n.s., not significant versus n.i. determined using one-way ANOVA with Tukey's multiple-comparison test. (C) Immunoblot analysis of SUMO1 and tubulin levels in lysates of control (AS), SENP1, or SENP2 siRNA-transfected A549 cells infected with Kp52145 for 5 h. AS, AllStars control, nonsilencing siRNA. SUMO1 smears were quantified from three independent experiments using Image Studio Lite (LI-COR) and normalized to α -tubulin. The graph represents fold change compared to AS-transfected noninfected control cells. n.s., not significant; ***, $P \leq 0.001$; *, $P \leq 0.05$ by one-way ANOVA with Bonferroni's multiple-comparison test. (D) Fluorescence microscopy of pSEN2-GFP-transfected A549 cells grown on glass coverslips. Cells were infected with Kp52145 for 5 h or left uninfected (n.i.). Coverslips were stained with Hoechst (4',6-diamidino-2-phenylindole [DAPI]) for nucleus identification. The percentage of SENP2 localized in either nucleus or cytoplasm is represented on the graph and is the result of independent counting of 100 cells from each of 3 independent experiments. (E) Immunoblot analysis of SENP2 and tubulin levels in cytosolic extracts of A549 cells infected with Kp52145 for 5 h or left uninfected. (F) Fluorescence microscopy of pSEN2-GFP transfected A549 cells grown on glass coverslips. Cells were treated with the proteasomal inhibitor MG262 (5 μ M, 2 h before infection), the nuclear export inhibitor leptomycin B (LMB; 10 nM, 2 h before infection), or DMSO (vehicle solution) and infected with Kp52145 for 5 h or left uninfected (n.i.). Coverslips were stained with Hoechst (DAPI) for nucleus identification. The percentage of SENP2 localized in either nucleus or cytoplasm is represented on the graphs and is the result of independent counting of 100 cells from each of 3 independent experiments. (G) Immunoblot analysis of SUMO1 (antibody sc-9060) and tubulin levels in lysates of the nuclear export inhibitor leptomycin B- (5 μ M, 2 h before infection) or DMSO (vehicle solution) and infected with Kp52145 for 5 h or left uninfected (n.i.). SUMO1 smears were quantified from three independent experiments using Image Studio Lite (LI-COR) and normalized to α -tubulin. The graph represents fold change compared to AS-transfected noninfected control cells. n.s., not significant; ***, $P \leq 0.001$; *, $P \leq 0.05$ by one-way ANOVA with Bonferroni's multiple-comparison test. (Continued on next page)

proteins in infected SENP2 knockdown cells compared to that in cells transfected with nonsilencing control siRNA (AS) and the other SENPs (Fig. 2C; see also Fig. S2A), suggesting that SENP2 mediates the decrease in conjugated SUMO1 proteins in *K. pneumoniae*-infected cells. Control experiments showed that *Klebsiella* infection did not alter the transcription of any SENPs (Fig. S2B).

Owing to the global scale of the SUMOylation decrease in infected cells, it was intriguing that SENP2, a nucleus-associated deSUMOylase (19), accounts for the *Klebsiella*-triggered decrease in SUMOylation. We then sought to determine whether *Klebsiella* might affect the cellular distribution of SENP2 in infected cells. Fluorescence-based single-cell analysis confirmed that SENP2-green fluorescent protein (GFP) was mostly localized in the nuclei of noninfected A549 cells (Fig. 2D). In contrast, SENP2-GFP was mostly localized in the cytosol of infected cells (Fig. 2D). This finding was further supported by immunoblotting of cytosolic extracts demonstrating an accumulation of endogenous SENP2 in infected cells (Fig. 2E).

In human bone osteosarcoma epithelial cells (U-2 OS), it has been shown that SENP2 shuttles continuously between the nucleus and the cytoplasm, where it is degraded by the 26S ubiquitin proteasome (20). Corroborating these findings, pretreatment of A549 cells with the proteasome inhibitor MG262 led to the accumulation of SENP2-GFP in the cytosol (Fig. 2F). The localization of SENP2-GFP in the cytosol of infected cells was abrogated when infections were performed in the presence of leptomycin B, a nuclear export inhibitor (Fig. 2F), demonstrating that the presence of SENP2 in the cytosol of infected cells is dependent on nucleocytoplasmic shuttling. The *Klebsiella*-induced decrease in SUMOylation was not observed in leptomycin B-treated cells (Fig. 2G), indicating that *Klebsiella*-triggered SENP2 localization in the cytosol mediates the decrease in the levels of SUMO-conjugated proteins.

***K. pneumoniae* triggers loss of cullin-1 NEDDylation to increase SENP2 levels.**

To gain molecular insights into how *Klebsiella* increases the levels of SENP2 in the cytosol of infected cells, we hypothesized that *K. pneumoniae* may compromise the ubiquitin proteasome-mediated degradation of SENP2 occurring in the cytosol (20). The fact that SENP2 ubiquitylation is a necessary event to mark the protein for degradation by the 26S proteasome (20) prompted us to assess whether SENP2 is ubiquitylated in infected cells. In MG262-treated cells, GFP-tagged SENP2 was pulled down with an anti-GFP antibody, and K48-conjugated SENP2 was detected with an anti-K48 antibody. Ubiquitylated SENP2 was barely detected in *Klebsiella* infected cells in contrast to that in noninfected cells (Fig. 2H), sustaining the notion that SENP2 accumulation in the cytosol of infected cells is due to reduced proteasomal degradation, because SENP2 is not K48 ubiquitin tagged.

We next sought to identify the E3 ubiquitin ligase complex responsible for SENP2 ubiquitylation. The SCF (S-phase-kinase-associated protein 1 [Skp1], Cullin-1 (Cul-1), F-box protein) E3 ubiquitin ligases are the largest family of E3s in mammals (21). Reduction in the levels of the adaptor protein Skp1 and the scaffold protein Cul-1 by siRNA led to an accumulation of SENP2 in the cytosol of noninfected cells (Fig. 2I). The

FIG 2 Legend (Continued)

infection) or DMSO (vehicle solution)-treated A549 infected with Kp52145 for 5 h or left uninfected. SUMO1 smears were quantified using Image Studio Lite (LI-COR) and normalized to α -tubulin. The graph represents fold change compared to DMSO noninfected control cells. ***, $P \leq 0.001$; **, $P \leq 0.01$; *, $P \leq 0.05$ by one-way ANOVA with Bonferroni's multiple-comparison test. (H) Immunoblot analysis of K48 linkage-specific polyubiquitin and GFP levels in immunoprecipitates of A549 infected with Kp52145 for 5 h. Cells were immunoprecipitated using anti-GFP antibody. Preimmune mouse IgG served as a negative control. (I) Immunoblot analysis of SENP2 and tubulin levels in cytosolic extracts of control (AS), RBX1, Skp1, Cul-1, β TrCP or Skp2 siRNA-transfected A549 cells left uninfected. (J) Immunoblot analysis of cullin-1 and tubulin levels in lysates of A549 cells infected with Kp52145 for 5 h or left uninfected. Lysates of A549 treated with 5 mM H_2O_2 for 10 min were used as a positive control for cullin-1 deNEDDylation. (K) Immunoblot analysis of Cul-1 and tubulin levels in lysates of control (AS) or CSN5 siRNA-transfected A549 cells infected with Kp52145 for 5 h or left uninfected. (L) Immunoblot analysis of K48 linkage-specific polyubiquitin and GFP levels in immunoprecipitates of control (AS) or CSN5 siRNA-transfected A549. Cells were transfected with a SENP2-GFP plasmid 24 h after the siRNA transfection and infected the following day with Kp52145 for 5 h or left uninfected. Cells were immunoprecipitated using anti-GFP antibody. Preimmune mouse IgG served as negative control. (M) Immunoblot analysis of SENP2 and tubulin levels in cytosolic extracts of control (AS) or CSN5 siRNA-transfected A549 cells infected with Kp52145 for 5 h or left uninfected. (N) Immunoblot analysis of SUMO1 and tubulin levels in lysates of control (AS) or CSN5 siRNA-transfected A549 cells infected with Kp52145 for 5 h or left uninfected. SUMO1 smears were quantified from three independent experiments using Image Studio Lite (LI-COR) and normalized to α -tubulin. The graph represents fold change compared to AS-transfected noninfected control cells. ***, $P \leq 0.001$; **, $P \leq 0.01$; *, $P \leq 0.05$ by one-way ANOVA with Bonferroni's multiple-comparison test. In all panels, data are representative of at least three independent experiments.

F-box protein determines the substrate specificity of the SCF, with three major classes of F-box proteins depending on the substrate interaction domain (WD40 repeats as β TrCP, leucine-rich repeats as Skp1 or Skp2, and other types such as cyclin F). siRNA-based experiments showed the accumulation of SENP2 only in the cytosol of β TrCP knockdown cells (Fig. 2I). Altogether, these results demonstrate that the SCF-E3 ligase Skp1-Cul-1- β TrCP mediates the degradation of SENP2 in the cytosol of cells.

The activity of SCF requires the conjugation of the ubiquitin-like polypeptide NEDD8 to Cul-1, suggesting the possibility that *Klebsiella* may trigger the loss of Cul-1 NEDDylation, resulting in the lack of transfer of ubiquitin to SENP2. Typically, Cul-1 appears as a doublet at \sim 85 and \sim 90 kDa, with the higher molecular band representing the NEDDylated form of Cul-1 (22). Immunoblotting experiments revealed the lack of Cul-1 NEDDylation in infected cells (Fig. 2J). As a positive control, cells were pretreated with H₂O₂, as this was shown to cause loss of Cul-1 NEDDylation (Fig. 2J) (23).

DeNEDDylation of Cul-1 is normally catalyzed by the COP9 signalosome (e.g., subunit 5 or CSN5/JAB1) (24). We then examined whether repression of CSN5 expression may inhibit *Klebsiella*-induced Cul-1 deNEDDylation. As shown in Fig. 2K, *Klebsiella*-triggered Cul-1 deNEDDylation was significantly reduced in CSN5 knockdown cells. In CSN5-silenced cells, *Klebsiella* did not reduce the K48-linked ubiquitylation of SENP2 (Fig. 2L), and, as anticipated, there was a reduction in SENP2 levels in the cytosol of infected cells (Fig. 2M). Finally, *Klebsiella* induced an increase in the global levels of SUMO1-conjugated proteins in CSN5-silenced cells (Fig. 2N).

In summary, these results demonstrate that *K. pneumoniae* impairs the cytosolic degradation of SENP2 by affecting its K48 ubiquitylation through CSN5-mediated deNEDDylation of the Cul-1 subunit of the SCF E3 ligase Skp1-Cul-1- β TrCP.

***K. pneumoniae* increases CSN5 levels through an EGFR-PI3K-AKT-ERK-GSK3 β pathway.** Transcription analysis showed that *K. pneumoniae* induced the expression of *csn5* in A549 cells (Fig. 3A), and immunoblotting experiments demonstrated that Kp52145 increased the levels of CSN5 (Fig. 3B). The regulation of CSN5 is poorly understood, although there is evidence showing that CSN5 is a target of EGFR signaling (25). Previous work from our laboratory revealed that *K. pneumoniae* activates the EGFR-phosphatidylinositol 3-kinase (PI3K)-protein kinase B (AKT)-extracellular signal-regulated kinase (ERK)-glycogen synthase kinase 3 beta (GSK3 β) signaling pathway to limit inflammation (14). We then investigated whether *Klebsiella*-induced expression of CSN5 is dependent on this signaling pathway. To test this hypothesis, we utilized pharmacologic inhibitors of EGFR (AG1478), PI3K (LY294002), AKT (AKT-X), or MEK (U0126) to block the pathway at four different levels. Immunoblotting revealed that Kp52145-triggered induction of CSN5 was reduced in cells pretreated with the inhibitors (Fig. 3C). Since we have shown that Kp52145 inactivates GSK3 β by triggering the phosphorylation of serine 9 (17), we examined the role of inhibitory phosphorylation of GSK3 β on CSN5 expression upon Kp52145 infection. Vectors encoding wild-type GSK3 β (GSK3 β -WT) or a constitutively active mutant (GSK3 β -S9A) in which the serine 9 residue was changed to alanine were transiently transfected into A549 cells. As a control, cells were transfected with the empty vector pcDNA3. *Klebsiella* did not induce CSN5 in cells transfected with the GSK3 β -S9A vector (Fig. 3C), demonstrating that the inhibitory phosphorylation of GSK3 β is required for *Klebsiella* induction of CSN5. Next, we examined whether inhibition of this EGFR-controlled signaling pathway would abrogate *Klebsiella*-imposed reduction in SUMOylation. Indeed, pretreatment of the cells with the EGFR inhibitor AG1478 led to an overall increase in SUMO1 levels upon infection (Fig. 3D). Because *Klebsiella* CPS is the bacterial factor triggering the activation of EGFR (14), we assessed whether *Klebsiella*-induced CSN5 upregulation is dependent on the CPS. As anticipated, the *cps* mutant, strain 52145 Δ wca_{K22}, did not increase CSN5 levels in A549 cells (Fig. 3E).

Overall, these findings support the notion that *Klebsiella* CPS engages an EGFR-PI3K-AKT-ERK-GSK3 β pathway to increase the levels of CSN5 to decrease the levels of SUMO-conjugated proteins.

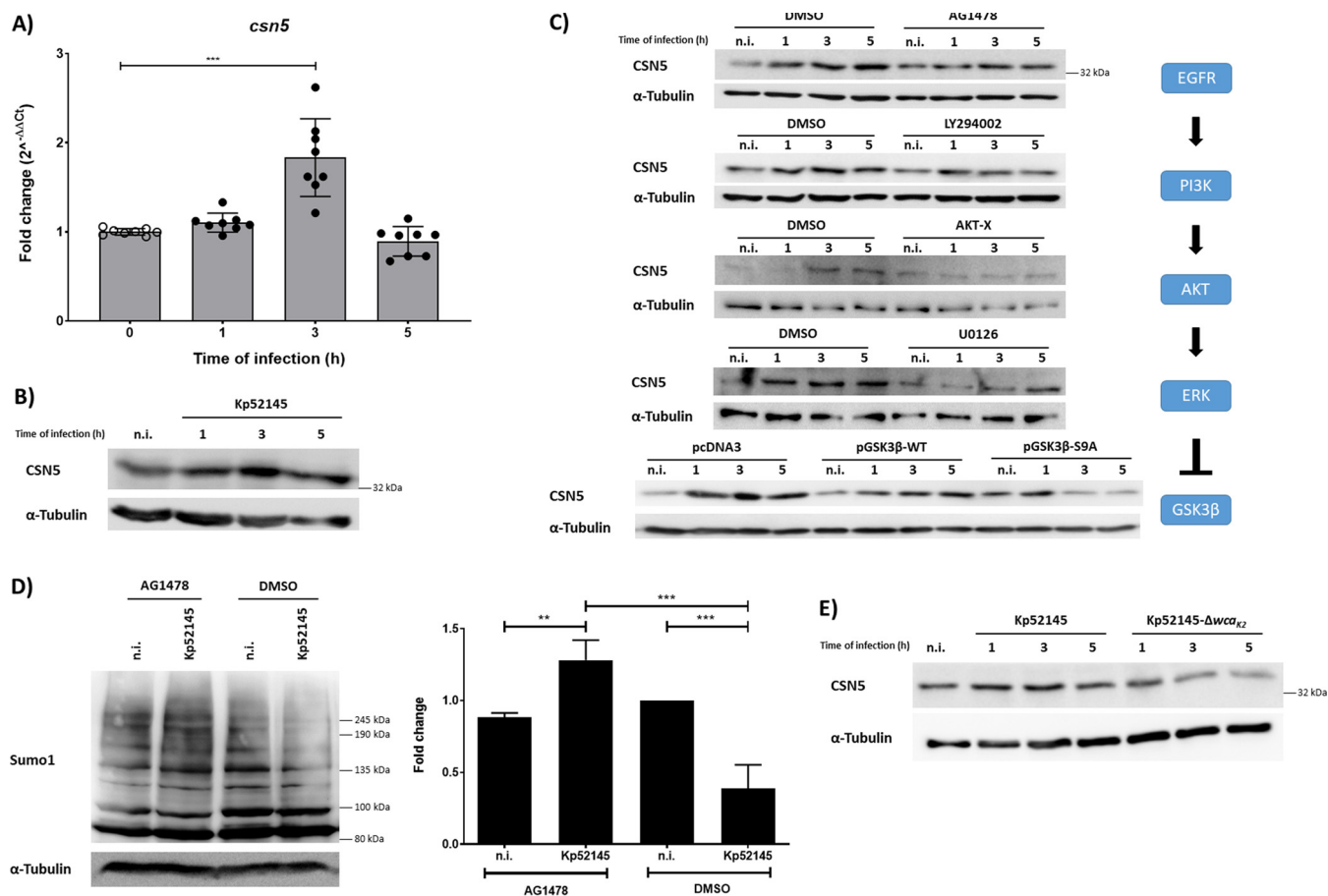


FIG 3 *K. pneumoniae* increases CSN5 levels in an EGFR-PI3K-AKT-ERK-GSK3 β -dependent manner. (A) *csn5* mRNA levels, assessed by qPCR, in A549 cells left untreated (n.i.) or infected for up to 5 h with Kp52145. Values are presented as the means \pm standard deviations (SDs) from three independent experiments measured in duplicates. ***, $P \leq 0.001$ by one-way ANOVA with Bonferroni's multiple-comparison test. (B) Immunoblot analysis of CSN5 and tubulin levels in lysates of A549 cells infected with Kp52145 for the indicated times. (C) Immunoblot analysis of CSN5 and tubulin levels in lysates of A549 cells infected with Kp52145 for the indicated times. Cells were pretreated with AG1478 (5 μ M), LY294002 (20 μ M), AKT-X (30 μ M), U0126 (10 μ M), or DMSO (vehicle solution) for 2 h before infection where indicated. Where indicated, cells were transfected with plasmids expressing GSK3 β either wild-type or with a S9A mutation that renders the protein constitutively active or with pcDNA3, empty vector. The signaling pathway EGFR-PI3K-AKT-ERK-GSK3 β activated in *K. pneumoniae* infection is depicted to represent the several steps inhibited in this figure. (D) Immunoblot analysis of SUMO1 levels in lysates of AG1478- (5 μ M, 2 h before infection) or DMSO (vehicle solution)-treated A549 cells infected with Kp52145 for the indicated times. Membranes were reprobed for tubulin as a loading control. SUMO1 smears were quantified from three independent experiments using Image Studio Lite (LI-COR) and normalized to α -tubulin. The graph represents fold change at 5 h of infection compared to DMSO noninfected control cells. **, $P \leq 0.01$; ***, $P \leq 0.001$ by one-way ANOVA with Bonferroni's multiple-comparison test. (E) Immunoblot analysis of CSN5 and tubulin levels in lysates of A549 cells infected with Kp52145 or 52145 Δwca_{K2} for the indicated times. In all panels, data are representative of at least three independent experiments.

***K. pneumoniae* decreases SUMOylation in macrophages.** Having demonstrated that *Klebsiella* reduces SUMOylation in epithelial cells, we investigated whether *Klebsiella* affects SUMO-conjugated proteins in macrophages. A wealth of evidence has established that macrophages play a crucial role in host defense against *K. pneumoniae*, not only by clearing the bacteria but also by shaping the immune response against this pathogen (26, 27). MH-S mouse alveolar macrophages were infected with Kp52145, and the overall pattern of SUMO1-conjugated proteins was accessed by immunoblotting. Figure 4A shows that Kp52145 induced a decrease in the levels of SUMO1-conjugated proteins as well as a decrease in the levels of free SUMO1 (Fig. 4B). Similar results were observed in infected THP-1 human macrophages (Fig. 4C), indicating that the decrease in SUMOylation is not cell type dependent. Either UV-killed or heat-killed bacteria did not trigger a decrease in the level of SUMOylated proteins (Fig. S3), demonstrating that the reduction in the levels of SUMOylated proteins is mediated by live bacteria.

Previous work from this laboratory demonstrated the importance of the *K. pneumoniae* polysaccharides, CPS and lipopolysaccharide (LPS), in the interplay between the

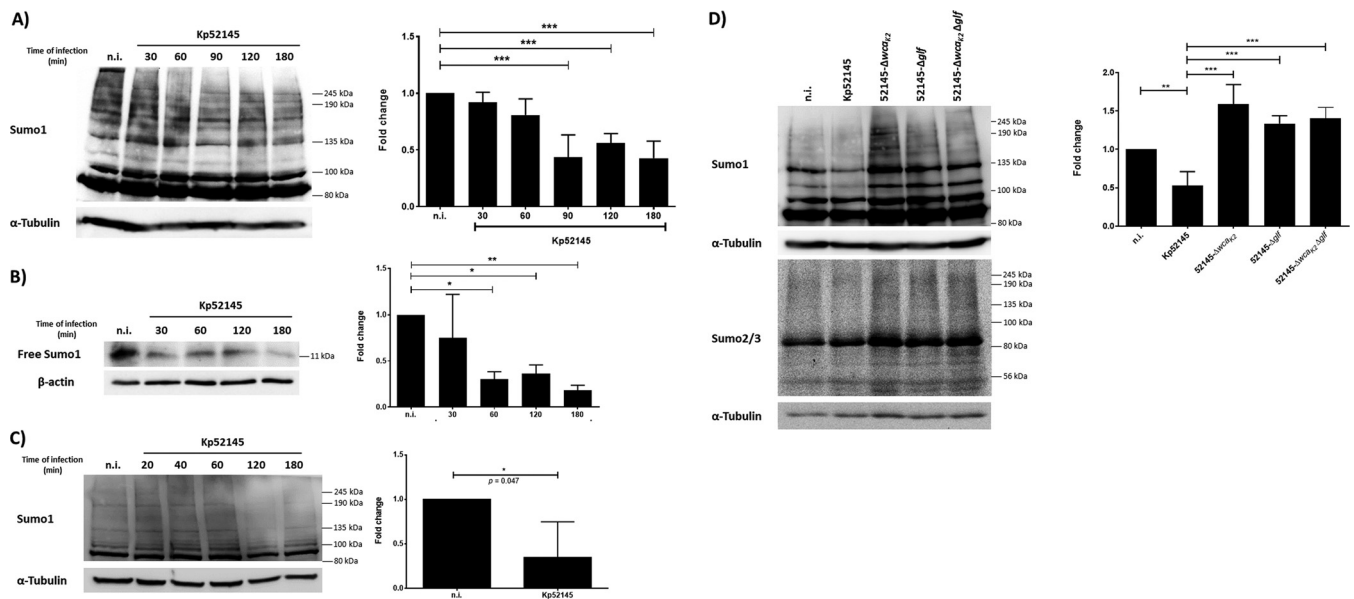


FIG 4 *K. pneumoniae* decreases SUMOylation in macrophages. (A) Immunoblot analysis of SUMO1 and tubulin levels in lysates of mouse alveolar macrophages, MH-S cells, infected with Kp52145 for the indicated time points. SUMO1 smears were quantified from three independent experiments using Image Studio Lite (LI-COR) and normalized to α -tubulin. The graph represents fold change compared to noninfected control cells at the indicated time points. ***, $P \leq 0.001$ by one-way ANOVA with Bonferroni's multiple-comparison test. (B) Immunoblot analysis of SUMO1 and tubulin levels in lysates of MH-S cells infected with Kp52145 for the indicated time points. The band corresponding to free SUMO1 at 11 kDa was quantified from three independent experiments using Image Studio Lite (LI-COR) and normalized to α -tubulin. The graph represents fold change compared to noninfected control cells at the indicated time points. *, $P \leq 0.05$; **, $P \leq 0.01$ by one-way ANOVA with Bonferroni's multiple-comparison test. (C) Immunoblot analysis of SUMO1 (antibody sc-9060) and tubulin levels in lysates of human monocyte THP-1 cells infected with Kp52145 for the indicated time points. SUMO1 smears were quantified from three independent experiments using Image Studio Lite (LI-COR) and normalized to α -tubulin. The graph represents fold change at 180 min compared to noninfected control cells. Two-tailed unpaired *t* test. (D) Immunoblot analysis of SUMO1 and tubulin levels in lysates of MH-S cells infected with Kp52145 or the indicated mutants for 1 h. SUMO1 smears were quantified from three independent experiments using Image Studio Lite (LI-COR) and normalized to α -tubulin. The graph represents fold change compared to noninfected control cells. **, $P \leq 0.01$; ***, $P \leq 0.001$ by one-way ANOVA with Bonferroni's multiple-comparison test. n.i., noninfected control. In all panels, data are representative of at least three independent experiments.

pathogen and macrophages (28). To examine whether CPS and LPS mediate the *Klebsiella*-triggered decrease in SUMOylation, we assessed the global pattern of SUMO1-conjugated proteins in macrophages infected with the CPS (52145 Δ wca_{K2}) and LPS O-polysaccharide (52145 Δ gff) mutants and the double mutant lacking both polysaccharides (52145 Δ wca_{K2} Δ gff). Immunoblotting revealed an increase in the levels of SUMO-conjugated proteins in macrophages infected with the CPS and LPS O-polysaccharide mutants (Fig. 4D), indicating that both polysaccharides have a role in the *Klebsiella*-triggered decrease in SUMOylated proteins. Controls confirmed there were no differences in the levels of surface-attached capsule produced by the wild-type and the LPS O-polysaccharide mutant (174.4 and 174.8 μ g glucuronic acid/ 10^{-9} CFU, respectively).

***K. pneumoniae*-induced decrease in SUMOylation in macrophages is mediated by TLR4-dependent type I interferon.** Like in epithelial cells, Ubc9 levels were not decreased in *Klebsiella*-infected macrophages (see Fig. S4A). Cell fractionation experiments did not reveal increased levels of SENP2 in the cytosol (Fig. S4B), and NEDDylation of Cul-1 was not impaired in infected macrophages (Fig. S4C). Collectively, these observations indicated that *Klebsiella* may employ a different strategy in macrophages to decrease the levels of SUMO1-conjugated proteins.

The fact that the CPS and LPS O-polysaccharide mediated the *Klebsiella*-triggered decrease in SUMOylated proteins and that both polysaccharides are recognized by TLR4 (13, 29) led us to investigate whether *Klebsiella* targets TLR4 signaling to decrease SUMOylation. We observed an increase in SUMOylated proteins in infected *tlr4*^{-/-} immortalized bone marrow-derived macrophages (iBMDMs) (Fig. 5A). TLR4 signals via adaptors MyD88 and TRIF, with TRAM acting as a sorting adaptor controlling TRIF localization (30). To learn which TLR4 adaptor(s) mediates the *Klebsiella*-induced

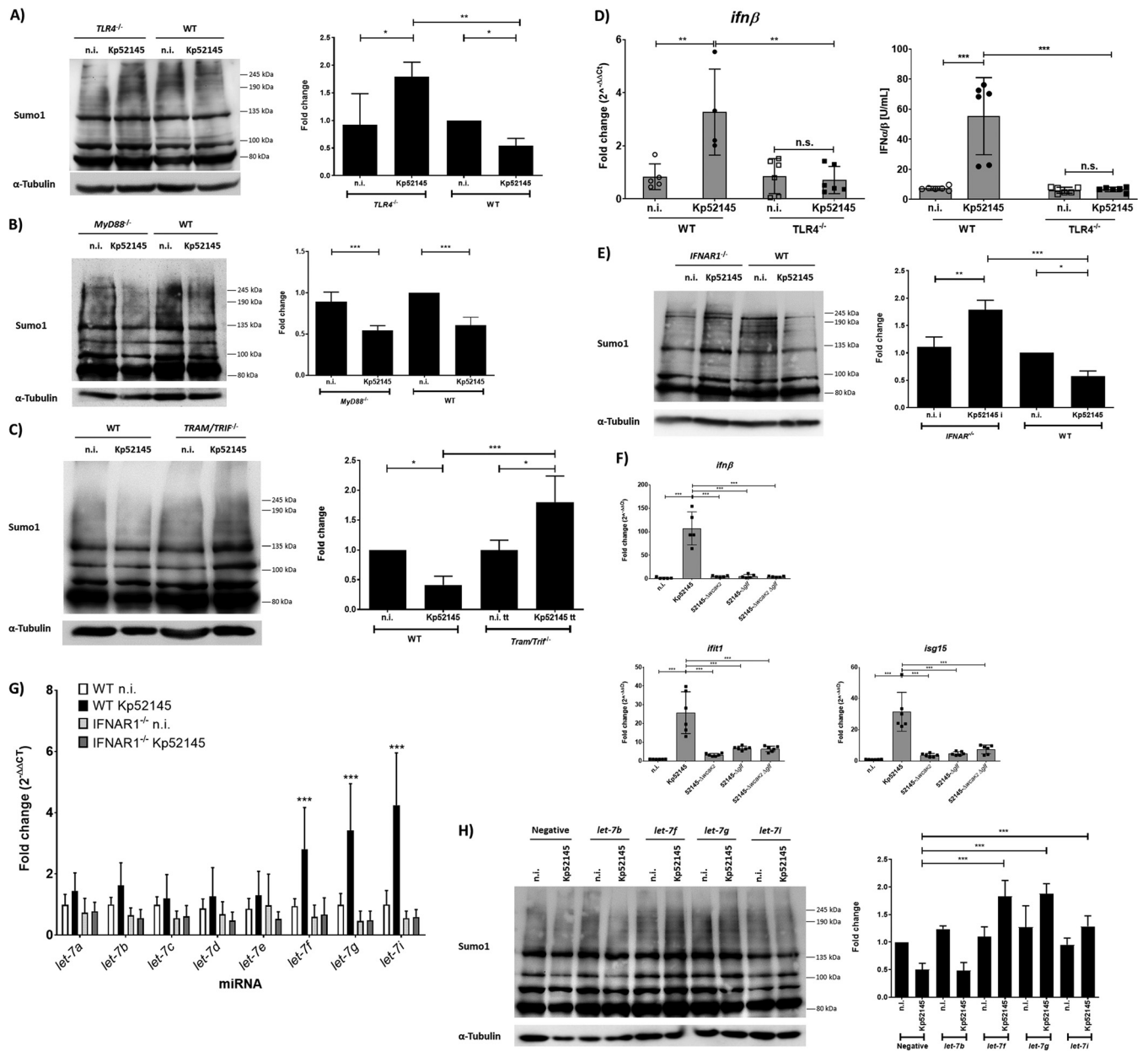


FIG 5 *K. pneumoniae* SUMOylation decrease in macrophages is mediated by TLR4-dependent type I interferon and *let-7* miRNAs. (A) Immunoblot analysis of SUMO1 and tubulin levels in lysates of immortalized bone marrow-derived macrophages (iBMDMs) derived from C57BL/6 mice (WT) or *Tlr4* knockout mice (*tlr4*^{-/-}) infected with Kp52145 for the indicated time points. SUMO1 smears were quantified from three independent experiments using Image Studio Lite (LI-COR) and normalized to α -tubulin. The graph represents fold change compared to wild-type (WT) iBMDM noninfected control cells. ***P* ≤ 0.01; **P* ≤ 0.05 by one-way ANOVA with Bonferroni's multiple-comparison test. (B) Immunoblot analysis of SUMO1 and tubulin levels in lysates of iBMDM cells derived from wild-type (WT) mice or MyD88 knockout mice (*myd88*^{-/-}) infected with Kp52145 for the indicated time points. SUMO1 smears were quantified from three independent experiments using Image Studio Lite (LI-COR) and normalized to α -tubulin. The graph represents fold change compared to wild-type (WT) iBMDM noninfected control cells. ****P* ≤ 0.001 by one-way ANOVA with Bonferroni's multiple-comparison test. (C) Immunoblot analysis of SUMO1 and tubulin levels in lysates of iBMDM cells derived from WT mice or TRAM/TRIF double knockout mice (*tram/trif*^{-/-}) infected with Kp52145 for the indicated time points. SUMO1 smears were quantified from three independent experiments using Image Studio Lite (LI-COR) and normalized to α -tubulin. The graph represents fold change compared to wild-type (WT) iBMDM noninfected control cells. ****P* ≤ 0.001; ***P* ≤ 0.01; **P* ≤ 0.05 by one-way ANOVA with Bonferroni's multiple-comparison test. (D) Type I IFN levels determined in the supernatants of iBMDM wild-type (WT) or *tlr4*^{-/-} cells left untreated (n.i.) or infected for 3 h with Kp52145. The reporter cell line B16-Blue IFN- α/β was used for the quantification of levels of SEAP produced upon stimulation of the supernatants with the detection medium QUANTI-Blue and presented as IFN- α/β U ml⁻¹. IFN- β mRNA levels were assessed by qPCR and are presented as fold change against untreated wild-type (WT) cell levels. Values are presented as the means \pm SDs from three independent experiments measured in duplicates. ****P* ≤ 0.001; ***P* ≤ 0.01; **P* ≤ 0.05; n.s., not significant by one-way ANOVA with Tukey's multiple-comparison test. (E) Immunoblot analysis of SUMO1 and tubulin levels in lysates of BMDM cells derived from wild-type (WT) or IFNAR1 knockout mice (*ifnar1*^{-/-}) infected with Kp52145 for the indicated time points or left untreated (n.i.). SUMO1 smears were quantified from three independent experiments using Image Studio Lite (LI-COR) and normalized to α -tubulin. The graph represents fold change compared to wild-type (WT) BMDM noninfected control cells. ****P* ≤ 0.001; ***P* ≤ 0.01; **P* ≤ 0.05 by one-way ANOVA with Bonferroni's multiple-comparison test. (F) *ifnb1*, *ifit1*, and *isg15* mRNA levels, assessed by qPCR, in MH-S cells left untreated (n.i.) or infected for 3 h with the *K. pneumoniae* strains indicated. Values are presented as the means \pm SDs from three independent experiments measured in duplicates. ****P* ≤ 0.001 by one-way ANOVA with Tukey's multiple-comparison test.

(Continued on next page)

decrease in global SUMOylation, *myd88*^{-/-} and *tram/trif*^{-/-} iBMDMs were infected. We observed no differences in the global levels of SUMO1-conjugated proteins between wild-type and *myd88*^{-/-} iBMDMs (Fig. 5B). In contrast, there was an increase in the levels of SUMOylated proteins in *tram/trif*^{-/-} iBMDMs (Fig. 5C), indicating that *Klebsiella*-triggered decrease in SUMOylation is dependent on TLR4-TRAM-TRIF signaling.

The TLR4-TRAM-TRIF signaling pathway governs type I IFN production (31), making it relevant to investigate whether the *Klebsiella*-induced decrease in SUMOylation is mediated by type I IFN. Further confirming recent findings of our laboratory (32), Kp52145 induced IFN- β , *ifnb1*, and interferon-stimulated genes (ISGs) in wild-type iBMDMs, but those were significantly reduced in *tlr4*^{-/-} cells (Fig. 5D; see also Fig. S5A). To demonstrate the contribution of type I IFN to the *Klebsiella*-triggered decrease in levels of SUMO-conjugated proteins, we infected BMDMs obtained from *ifnar1*^{-/-} mice. Kp52145 increased the levels of SUMOylated proteins in *ifnar1*^{-/-} BMDMs (Fig. 5E), demonstrating that the *Klebsiella*-induced decrease in SUMOylation is indeed dependent on type I IFN signaling. We then investigated whether a reduced induction of type I IFNs by the CPS and LPS O-polysaccharide mutants may explain the high levels of SUMO1-conjugated proteins in infected macrophages. Indeed, the three mutants induced less *ifnb1* and ISGs *ifit1* and *isg15* expression than the wild type (Fig. 5F). Furthermore, addition of type I IFN to macrophages infected with the double mutant lacking CPS and LPS O-polysaccharide rescued the decrease in the levels of SUMOylated proteins (Fig. S5B). Altogether, these findings provide compelling evidence to the notion that TLR4-TRAM-TRIF-induced type I IFN via IFN receptor 1 (IFNAR1)-controlled signaling mediates the *Klebsiella*-triggered decrease in the levels of SUMOylation.

let-7 miRNAs mediate type I IFN-mediated decrease in SUMOylation. IFNs regulate the expression of miRNAs from the *let-7* family (33). miRNAs downregulate mRNA stability and protein synthesis through complementary elements in the 3' untranslated regions (UTRs) of their target mRNAs. Sahin and coworkers reported that type I IFNs control SUMO expression and validated *let-7* target sequences in 3' UTRs of human and mouse *sumo1*, *sumo2*, and *sumo3* transcripts (34), indicating an evolutionary conserved regulation of SUMO by *let-7* family members. This evidence prompted us to investigate whether the *Klebsiella*-induced decrease in the overall levels of SUMO-conjugated proteins by type-I IFNs is through *let-7* miRNAs. We reasoned that Kp52145 should upregulate the expression of a *let-7* miRNA member(s) only in wild-type but not in *ifnar1*^{-/-} BMDMs. Figure 5G shows that *Klebsiella* upregulated the expression of *let-7f*, *let-7g*, and *let-7i* in wild-type BMDMs. These miRNAs were not upregulated in *Klebsiella*-infected *ifnar1*^{-/-} BMDMs (Fig. 5G), leading us to study whether these *let-7* family members mediate the type I IFN-controlled decrease in SUMOylation in *Klebsiella*-infected macrophages. To validate this hypothesis, antagomirs for these *let-7* family members were transfected into macrophages, and the global pattern of SUMOylation was determined by immunoblotting. As controls, we also tested a nontargeting control antagomir and a *let-7b* antagomir, since this miRNA was not significantly upregulated by *Klebsiella* in wild-type BMDMs (Fig. 5G). In contrast to cells transfected with a nontargeting control, inhibition of *let-7f*, *let-7g*, and *let-7i* led to a global upregulation of SUMOylation in infected cells (Fig. 5H). The effect was less prominent in *let-7i*-inhibited cells than in *let-7f* and *let-7g* ones (Fig. 5H). Collectively, these results reveal that *Klebsiella*-dependent type I IFN-mediated decrease in SUMOylation involves *let-7* miRNAs.

FIG 5 Legend (Continued)

(G) *let-7* mRNA levels, assessed by qPCR, in BMDM cells derived from wild-type (WT) or *ifnar1*^{-/-} mice infected with Kp52145 for 1 h or left untreated (n.i.). Values are presented as the means \pm SDs from three independent experiments measured in duplicates. ***, $P \leq 0.001$ versus WT n.i. determined using two way-ANOVA with Holm-Sidak's multiple-comparison test. (H) Immunoblot analysis of SUMO1 and tubulin levels in lysates of *let-7* miRNA antagomir-transfected MH-S cells infected with Kp52145 for 1 h or left untreated (n.i.). Negative, *Caenorhabditis elegans* control sequence with minimal sequence identity in mouse cells. SUMO1 smears were quantified from three independent experiments using Image Studio Lite (LI-COR) and normalized to α -tubulin. The graph represents fold change compared to negative-transfected noninfected control cells. ***, $P \leq 0.001$ by one-way ANOVA with Bonferroni's multiple-comparison test. In panels A, B, C, E, and H, data are representative of at least three independent experiments.

SUMOylation increases host defenses against *K. pneumoniae*. The sophisticated strategies employed by *Klebsiella* to decrease the levels of SUMO-conjugated proteins in epithelial cells and macrophages strongly suggested that SUMOylation should play an important role in host defense against *Klebsiella* infections. Therefore, we sought to determine whether alterations in the levels of SUMO1-conjugated proteins might influence *Klebsiella*-cell cross talk. By using a SUMO1 expression plasmid, a common method to upregulate the SUMO status of the host proteins (5, 6), we transiently upregulated SUMOylation (see Fig. S6A and B). We and others have established that the dampening of inflammation is a hallmark of *Klebsiella* infection biology *in vitro* and *in vivo* (12, 14, 15, 35, 36). Therefore, we examined the levels of interleukin 8 (IL-8) and tumor necrosis factor alpha (TNF- α) released by infected epithelial cells and macrophages, respectively. IL-8 and TNF- α are well-established inflammatory readouts upon infection. In SUMO1-overexpressing A549 cells, we observed a significant increase in IL-8 in the supernatants of infected cells (Fig. 6A). Furthermore, knockdown of SENP2 also led to increased release of IL-8, strengthening the role of this protein in controlling SUMOylation levels and inflammation (Fig. 6B). SUMO1-overexpressing macrophages also produced more TNF- α upon infection (Fig. 6C). Interestingly, macrophages transfected with *let-7f* and *let-7g* antagomirs also released more TNF- α upon infection (Fig. 6D), further sustaining the connection between increased SUMOylation and inflammation in macrophages. Collectively, these findings suggest that the *Klebsiella*-triggered decreased in SUMOylation in epithelial cells and macrophages is a pathogen strategy to limit inflammation.

To further investigate this notion, we examined the activation of NF- κ B and MAP kinases by *Klebsiella*. NF- κ B and MAP kinases govern the expression of inflammatory markers upon *Klebsiella* infection (13, 15). In the canonical NF- κ B activation pathway, nuclear translocation of NF- κ B is preceded by phosphorylation and subsequent degradation of I κ B α . I κ B α levels were reduced in SUMO1-overexpressing infected epithelial cells and macrophages (Fig. 6E). No significant differences in the phosphorylation of MAPKs were observed (Fig. 6F), indicating that the activation status of MAPKs upon *Klebsiella* infection is not affected by SUMOylation. The inhibition of the canonical NF- κ B pathway with BAY 11-7082 (an inhibitor of cytokine-induced I κ B α phosphorylation) led to a marked decrease of cytokine release in SUMO1-overexpressing cells (Fig. 6G), connecting the increased release of inflammatory mediators in SUMO1-overexpressing cells with the activation of NF- κ B.

Recently, we demonstrated that *K. pneumoniae* survives inside macrophages residing in the *Klebsiella*-containing vacuole (37). To learn whether SUMOylation plays any role in *Klebsiella* intracellular survival, SUMO1-overexpressing macrophages were infected, and the number of intracellular bacteria was determined 3 h postinfection. Figure 6H shows that the number of intracellular bacteria was significantly reduced in cells overexpressing SUMO. *Klebsiella* attachment was not affected in SUMO1-overexpressing cells (Fig. S6C), indicating that an increase in SUMOylation is detrimental for *K. pneumoniae* intracellular survival. Further sustaining this notion, we observed a significant decrease in bacterial numbers in macrophages transfected with *let-7f* and *let-7g* antagomirs (Fig. 6I). *Klebsiella* attachment was not affected in antagomir-transfected cells (Fig. S6D), demonstrating the importance of *Klebsiella*-induced *let-7* family members for intracellular survival.

Overall, these data provide evidence that a *Klebsiella*-induced decrease in SUMOylation promotes bacterial infection.

DISCUSSION

SUMOylation is a conserved process in the eukaryotic kingdom. In humans, thousands of SUMOylated proteins have been identified, and they are involved in transcription regulation, stress responses, and cell intrinsic immunity among many other biological processes (1). Consistent with the essential role of SUMOylation in the host cell, it has been shown that pathogens can interfere with this PTM to promote their own survival and replication. The vast majority of evidence refers to how viruses target

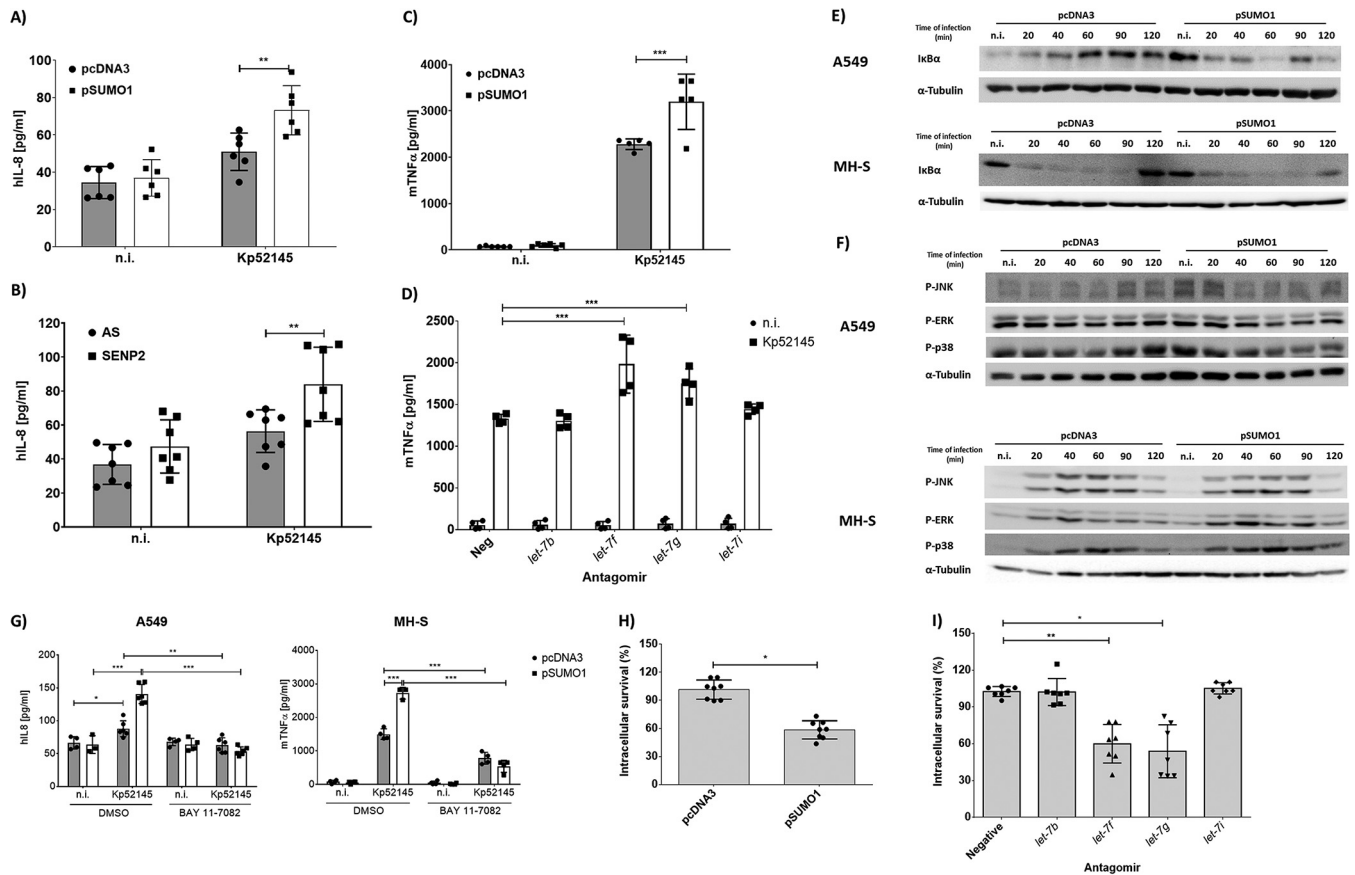


FIG 6 SUMOylation increases host defenses against *K. pneumoniae*. (A) ELISA of IL-8 secreted by A549 cells transfected with either empty control plasmid (pcDNA3) or SUMO1-hemagglutinin (HA) tag plasmid (pSUMO1), which were left untreated (n.i.) or infected with Kp52145 for 3 h of contact, after which, the medium was replaced with medium containing gentamicin ($100 \mu\text{g ml}^{-1}$) to kill extracellular bacteria and incubated for a further 4 h. Values are presented as the means \pm SDs from three independent experiments measured in duplicates. **, $P \leq 0.01$ by two-way ANOVA with Holm-Sidak's multiple-comparison test. (B) ELISA of IL-8 secreted by control (AS) or SENP2 siRNA-transfected A549, which were left untreated (n.i.) or infected with Kp52145 for 3 h of contact, after which, the medium was replaced with medium containing gentamicin ($100 \mu\text{g ml}^{-1}$) to kill extracellular bacteria and incubated for a further 4 h. Values are presented as the means \pm SDs from three independent experiments measured in duplicates. **, $P \leq 0.01$ by two-way ANOVA with Holm-Sidak's multiple-comparison test. (C) ELISA of TNF- α secreted by empty control (pcDNA3) or SUMO1-HA plasmid-transfected MH-S, which were left untreated (n.i.) or infected with Kp52145 for 1 h of contact, after which, the medium was replaced with medium containing gentamicin ($100 \mu\text{g ml}^{-1}$) to kill extracellular bacteria and incubated for a further 4 h. Values are presented as the means \pm SDs from three independent experiments measured in duplicates. ***, $P \leq 0.001$ by two-way ANOVA with Holm-Sidak's multiple-comparison test. (D) ELISA of TNF- α secreted by antagomir-transfected MH-S, which were left untreated (n.i.) or infected with Kp52145 for 1 h of contact, after which, the medium was replaced with medium containing gentamicin ($100 \mu\text{g ml}^{-1}$) to kill extracellular bacteria and incubated for a further 4 h. Values are presented as the means \pm SDs from three independent experiments measured in duplicates. ***, $P \leq 0.001$ by two-way-ANOVA with Holm-Sidak's multiple-comparison test; Neg, negative control. (E) Immunoblot analysis of I κ B α and tubulin levels in lysates of empty (pcDNA3) or SUMO1-HA (pSUMO1) plasmid transfected A549 or MH-S cells, infected with Kp52145 for the indicated time points. (F) Immunoblot analysis of phosphorylated Jun N-terminal protein kinase (P-JNK), P-ERK, and P-p38 levels in lysates of pcDNA3- or pSUMO1-transfected A549 or MH-S cells infected with Kp52145 for the indicated time points. Tubulin immunoblotting was used as the loading control. n.i., noninfected control. (G) ELISA of IL-8 or TNF- α secreted by empty control (pcDNA3) or SUMO1-HA plasmid-transfected A549 or MH-S, respectively, which were treated with the NF- κ B inhibitor BAY 11-7082 ($5 \mu\text{M}$, 2 h before infection) or DMSO (vehicle solution). Cells were left untreated (n.i.) or infected with Kp52145 for 1 h (MH-S) or 3 h (A549) of contact, after which, the medium was replaced with medium containing gentamicin ($100 \mu\text{g ml}^{-1}$) to kill extracellular bacteria and incubated for a further 4 h. Values are presented as the means \pm SDs from three independent experiments measured in duplicates. ***, $P \leq 0.001$; **, $P \leq 0.01$; *, $P \leq 0.05$ by two-way ANOVA with Holm-Sidak's multiple-comparison test. (H) Percent intracellular survival in MH-S cells transfected with either empty control plasmid (pcDNA3) or SUMO1-HA tag plasmid (pSUMO1). Cells were infected with Kp52145 for 30 min (MOI, 100:1), and wells were washed and incubated with medium containing gentamicin ($100 \mu\text{g ml}^{-1}$) for 2.5 h. Intracellular bacteria were quantified by lysis, serial dilution, and viable counting on LB agar plates. Percent intracellular survival was determined by dividing the number of CFU obtained at 3 h of infection over the number obtained at 1 h and considering pcDNA3 as 100%. Values are presented as the means \pm SDs from three independent experiments measured in duplicates. *, $P \leq 0.05$ by unpaired t test with correction for Holm-Sidak's multiple-comparison test. (I) Percent intracellular survival in antagomir-transfected MH-S cells. Cells were infected with Kp52145 for 30 min (MOI, 100:1), and wells were washed and incubated with medium containing gentamicin ($100 \mu\text{g ml}^{-1}$) for 2.5 h. Intracellular bacteria were quantified by lysis, serial dilution, and viable counting on LB agar plates. Percent intracellular survival was determined by dividing the number of CFU obtained at 3 h of infection over the number obtained at 1 h and considering the negative control as 100%. Values are presented as the means \pm SDs from three independent experiments measured in duplicates. **, $P \leq 0.01$; *, $P \leq 0.05$ by one-way ANOVA with Holm-Sidak's multiple-comparison test. In panels E and F, data are representative of at least three independent experiments.

SUMOylation (4), whereas little is known concerning the interplay between bacteria and this PTM. In this work, we demonstrate that the human pathogen *K. pneumoniae* induces a decrease in SUMOylation in epithelial cells and macrophages for intracellular survival and to limit the activation of inflammatory responses. Mechanistically, our

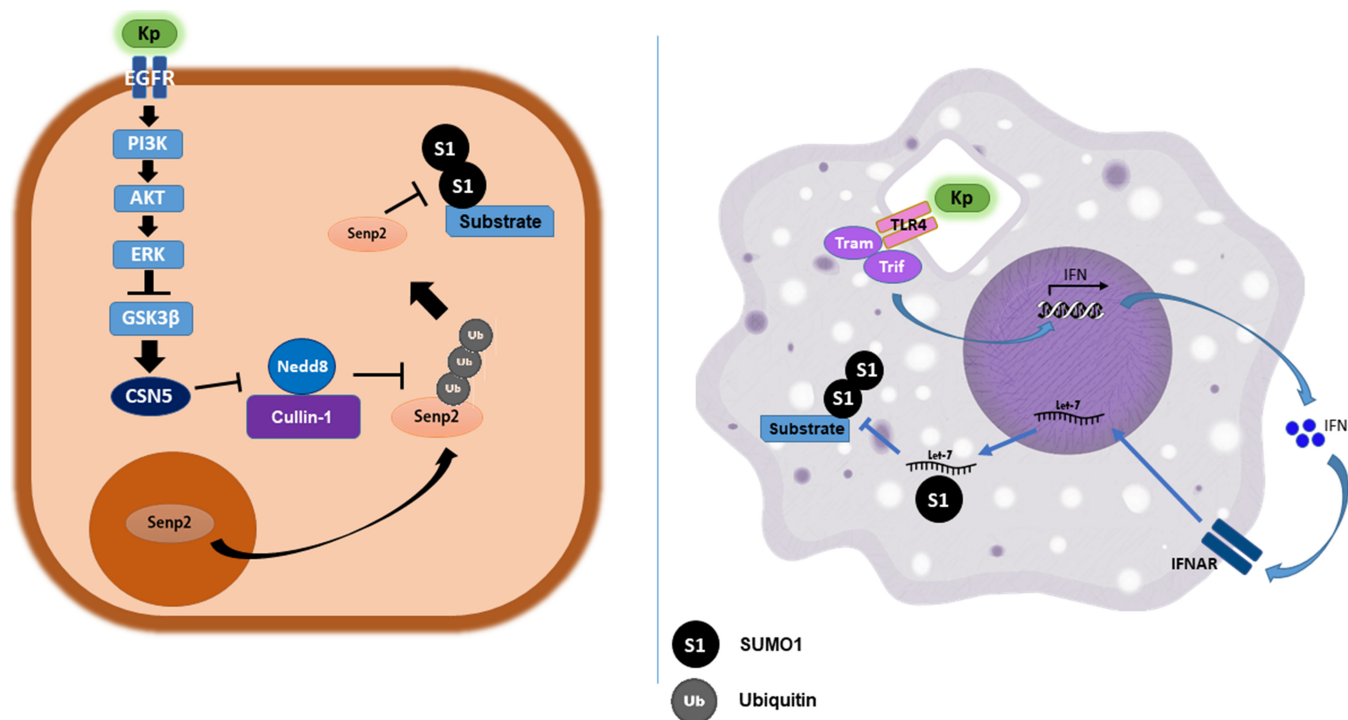


FIG 7 *Klebsiella pneumoniae* ablates SUMOylation via distinct pathways in epithelial cells or macrophages. Working model of *K. pneumoniae* strategies to decrease SUMOylation in epithelial cells and macrophages. In epithelial cells, Kp52145 activates the signaling pathway EGFR-PI3K-AKT-ERK-GSK3 β to increase the COP9 signalosome component CSN5, which inhibits NEDDylation of Cullin-1 and prevents proteasomal degradation of SENP2. SENP2 then accumulates in the cytosol, preventing SUMOylation. In macrophages, Kp52145 via TLR4-TRAM-TRIF induces the production of type I interferon, which signals through IFNAR1. Type I interferon stimulates transcription of the miRNA *let-7*, which prevents SUMOylation. Both strategies lead to increased intracellular survival and subversion of host responses.

findings uncover hitherto unknown strategies exploited by a pathogen to interfere with SUMOylation (Fig. 7). In epithelial cells, *K. pneumoniae* hijacks the SENP2 deSUMOylase, whereas in macrophages, *Klebsiella* exploits type I IFN-induced *let-7* miRNA to alter SUMOylation.

Our results in epithelial cells are reminiscent of those reported for the intracellular pathogens *L. monocytogenes*, *S. flexneri*, and *S. Typhimurium* that, like *Klebsiella*, decrease the levels of SUMO-conjugated proteins. Mechanistically, these pathogens induce the degradation of the E1 enzyme SAE2 and E2 enzyme Ubc9 to decrease SUMOylation (5–8). On the other hand, some bacterial effectors can mimic host deSUMOylases, such as the *Xanthomonas euvesicatoria* XopD (38) or the *Yersinia pestis* YopJ (39). However, and to the best of our knowledge, *Klebsiella*, a pathogen that does not invade epithelial cells, is the first among viral and bacterial pathogens exploiting a host deSUMOylase to reduce SUMOylation. Given the global decrease in levels of SUMO1-conjugated proteins triggered by *Klebsiella*, it was puzzling to identify the nucleus-associated deSUMOylase SENP2 as the deSUMOylase targeted by the pathogen. Several lines of evidence sustained that *Klebsiella* prevents the ubiquitin proteasome-dependent degradation of SENP2 to increase its levels in the cytosol to decrease SUMOylation. Our results conclusively demonstrate that *Klebsiella* targets NEDDylation, another PTM, to abrogate the K48-linked ubiquitylation of SENP2. To date, only commensal nonpathogenic bacteria have been shown to trigger the loss of NEDDylated Cul-1 in epithelial cells via generation of reactive oxygen species, which affect the function of the E2 enzyme Ubc12 (23); whereas the CHBP and Cif type 3 secretion effectors from *Burkholderia pseudomallei* and enteropathogenic *Escherichia coli*, respectively, trigger the deamidation of NEDD8 to abolish the ubiquitin ligase activity of the E3 ubiquitin ligase complex (37). In contrast, *Klebsiella*-induced lack of NEDDylation of Cul-1 was dependent on the CSN5 deNEDDylase. Our findings demonstrate that

Klebsiella induces CSN5 in an EGFR-PI3K-AKT-ERK-GSK3 β pathway-dependent manner. Interestingly, *Klebsiella* activates this pathway to blunt inflammation by inducing the expression of the deubiquitylase CYLD to limit the ubiquitylation of TRAF6 (15), placing this EGFR-governed pathway at the fulcrum of *Klebsiella* strategies to control PTMs to promote infection.

The fact that NEDDylation of Cul-1 is essential for the function of the ubiquitin ligase complex E3-SCF- β TrCP that controls the levels of proteins involved in host-pathogen interactions such as p53, β -catenin, and I κ B α among many others (40), warrants future studies to investigate the levels of proteins controlled by regulated proteolysis in *Klebsiella*-infected epithelial cells. Interestingly, recent proteomic analyses have revealed the NEDDylation of several hundreds of proteins (41). It is beyond the scope of this work to assess the impact of *K. pneumoniae* on the NEDDylation of proteins other than Cul-1. However, and based on the results of this work, we hypothesize that *Klebsiella* may decrease global NEDDylation, which may also contribute to the panoply of strategies developed by *Klebsiella* to manipulate host cell biology.

A common theme of the interplay between *K. pneumoniae* and epithelial cells emerges from this work and previous studies from our laboratory (14, 15). Here, we have shown that *Klebsiella* hijacks two proteins, SENP2 and CSN5, crucial to allow reversible conjugation of SUMO1 and NEDD8, respectively, to target proteins. Previously, we demonstrated that *Klebsiella* blocks the activation of NF- κ B and MAPK signaling pathways via the deubiquitinase CYLD and the phosphatase MKP-1, respectively, by preventing the ubiquitylation and phosphorylation of key signaling molecules (15). Cells activate CYLD and MKP-1 to return to homeostasis after inflammation to protect the host from an overwhelming inflammatory response (42, 43). Therefore, the picture that is taking shape is that a signature of *K. pneumoniae* infection biology is interfering with PTMs by hijacking host proteins used by the cells to return to homeostasis. This strategy is radically different from that employed by other pathogens, such as *Listeria*, *Salmonella*, *Shigella*, or *Mycobacterium*, who deliver bacterial proteins into host cells to modulate PTMs.

Another novel finding of this work is that *K. pneumoniae* interfered with SUMOylation in macrophages. Despite the crucial role played by macrophages in host defense and tissue homeostasis, there is limited evidence of pathogen-mediated alteration of PTMs in this cell type other than phosphorylation and ubiquitylation of proteins involved in the control of inflammatory responses. In this work, we have uncovered that the *Klebsiella*-triggered decrease of SUMOylation was dependent on TLR4-TRAM-TRIF-induced type I IFN. Whereas the role of SUMOylation governing IFN production during viral infection is well appreciated (44), we are not aware of any pathogen exploiting type I IFN to decrease the levels of SUMO-conjugated proteins. In fact, the role of type I IFNs in bacterial infections is still poorly understood (31), playing an adverse role in certain bacterial infections, while in others, type I IFNs are critical for host defense. In any case, our findings further expand the regulatory functions of type I IFNs beyond the control of innate and adaptive immune responses (45). Our results support the concept that the decrease in SUMOylation dependent on *Klebsiella*-induced type I IFN involves the upregulation of *let-7* miRNAs. This result is in line with previous studies showing posttranscriptional regulation of SUMO levels by *let-7* miRNA family members. It is interesting to note that depletion of Ubc9 by *S. Typhimurium* relies on upregulation of the small noncoding RNAs *miR-30c* and *miR-30e* (6), whereas Epstein-Barr virus-harbored miRNAs target several members of the SUMO interactome (46). It is therefore tempting to speculate that posttranscriptional regulation of components of the SUMOylation cascade might be a general strategy shared by pathogens to decrease SUMOylation. Some miRNAs, including *miR-146*, *miR-155*, *miR-125*, *let-7*, and *miR-21*, are commonly affected during bacterial infection to modulate host inflammatory responses (47). Interestingly, evidence indicates that downregulation of *let-7* is a conserved response shared by different pathogens to sustain inflammation (47, 48). In stark contrast, here we have shown that *K. pneumoniae* upregulates the expression of *let-7* miRNA family members in a type I IFN-dependent manner. Moreover, abrogation

of these miRNAs by transfecting specific antagomirs resulted in increased inflammatory responses and decreased intracellular survival in macrophages, supporting the notion that *K. pneumoniae* exploits *let-7* miRNA to manipulate host pathways. Future studies are warranted to develop a more comprehensive understanding of the roles of miRNAs in the *Klebsiella*-host interplay.

We were keen to identify the *K. pneumoniae* factor(s) mediating the *Klebsiella*-triggered decrease in SUMOylation. Our results revealed the crucial role played by *Klebsiella* polysaccharides, the CPS and the LPS O-polysaccharide, to decrease the levels of SUMO-conjugated proteins. The CPS and LPS are perhaps two of the best-characterized virulence factors of *K. pneumoniae*; the findings of our work expand the roles of these polysaccharides to counteract host defense responses. Importantly, these polysaccharides are required for *K. pneumoniae* survival in mice (pneumonia model) (12, 49, 50), underlining the importance of SUMOylation reduction as a *Klebsiella* virulence trait, since this process is abrogated in these mutant strains. In epithelial cells, CPS limits SUMOylation by preventing bacterial internalization and increasing the levels of the deNEDDylase CSN5. Notably, changes in the global pattern of SUMO-conjugated proteins in *Listeria* and *Shigella* infection affect the internalization of bacteria (5, 51); in *Klebsiella* infection, internalization of the *cps* mutant is associated with an increase in SUMOylation in epithelial cells. The fact that *Klebsiella*, *Listeria*, and *Shigella* decrease SUMOylation over time (5, 48) suggests that the proteins SUMOylated upon invasion may play an important role in host defense. Proteomic studies interrogating the SUMOylome after infection with different pathogens may lead to the identification of these proteins. Our results revealed that the CPS and LPS O-polysaccharide mediated the *Klebsiella*-triggered decrease in SUMOylation in macrophages in a TLR4-dependent manner. This is in perfect agreement with previous findings demonstrating that TLR4 recognizes both *K. pneumoniae* polysaccharides (13, 29). The conventional wisdom indicates that TLR signaling is crucial for host defense, whereas our findings demonstrate that pathogens can evolve to hijack TLR-governed signaling to attenuate host defenses, thus revealing a new angle in the host-pathogen arms race. Our findings are conceptually different from previously described antagonistic strategies of TLR signaling by pathogens to avoid activation of innate immune receptors (52). We recently demonstrated that *Klebsiella* targets another pathogen recognition receptor, NOD1, to attenuate the activation of NF- κ B-controlled inflammation, suggesting that manipulation of pathogen recognition receptors is one of the key features of *K. pneumoniae* anti-immune strategies (15). Collectively, we put forward the notion that hijacking the activation of immune receptors to promote virulence is an emerging theme in the infection biology of pathogens. Providing further support to this notion, Arpaia and coworkers have recently shown that *S. Typhimurium* requires cues from TLR-controlled signaling to regulate virulence genes necessary for intracellular survival, growth, and systemic infection (53).

A common theme for the battle of the host SUMO system versus bacterial pathogens emerges from the discoveries of this work and other recent publications investigating the interplay between SUMOylation and *Listeria*, *Salmonella*, and *Shigella* (5–8, 51). The message is that regardless of the molecular mechanisms employed to reduce SUMOylation, the outcomes are identical, i.e., the global decrease of SUMO-conjugated proteins. Future studies are warranted to identify the set of SUMOylated proteins playing a crucial role in host defense against *Klebsiella* and whether these are common to the other infections. It is tempting to consider that inhibition of deSUMOylation strategies could be a viable strategy to boost human defense mechanisms. This is challenging, as the evidence suggests that each pathogen uses different molecular mechanisms to abrogate SUMOylation, making it difficult to develop broad-spectrum therapeutics. In turn, an intriguing and exciting option to us is to develop drugs that increase SUMOylation. The targeting of SUMOylation is already being considered to develop new therapeutics against cancer and heart failure (54–56). Therefore, and based on the results shown here, it is well worth exploring the option of testing such drugs to treat bacterial infections.

MATERIALS AND METHODS

Cell culture. Lung epithelial A549 cells (ATCC CCL-185), murine alveolar MH-S macrophages (ATCC CRL-2019), and human THP-1 monocytes (ATCC TIB-202) were grown in RPMI 1640 medium (Gibco 21875) supplemented with 10% heat-inactivated fetal calf serum (FCS), 10 mM HEPES (Sigma), 100 U ml⁻¹ penicillin, and 0.1 mg ml⁻¹ streptomycin (Gibco) at 37°C in a humidified 5% CO₂ incubator.

The human airway epithelial cell line NuLi-1 (ATCC CRL-4011) was grown in bronchial epithelial cell basal medium (BEBM; Lonza CC-3171) with BEGM SingleQuot kit supplements and growth factors (Lonza CC-4175). Flasks and plates were coated with collagen type IV from placenta (Sigma C-7521).

Immortalized BMDMs (iBMDMs) from wild-type (WT), *tlr4*^{-/-}, *myd88*^{-/-}, and *tram/trif*^{-/-} mice on a C57BL/6 background were obtained from BEI Resources (NIAID, NIH) (repository numbers NR-9456, NR-9458, NR-15633, and NR-9568, respectively). iBMDM cells were grown in Dulbecco's modified Eagle medium (DMEM; Gibco 41965) supplemented with 10% heat-inactivated FCS, 100 U ml⁻¹ penicillin, and 0.1 mg ml⁻¹ streptomycin (Gibco) at 37°C in a humidified 5% CO₂ incubator.

Cells were routinely tested for *Mycoplasma* contamination. To isolate BMDMs (bone marrow-derived macrophages), tibias and femurs from C57BL/6 or *ifnar1*^{-/-} mice (C57BL/6 background) were removed using a sterile technique, and the bone marrow was flushed with fresh medium. To obtain macrophages, cells were plated in DMEM supplemented with filtered L929 cell supernatant (a source of macrophage colony-stimulating factor [M-CSF]) and maintained at 37°C in a humidified atmosphere of 5% CO₂ for 4 days. Medium was replaced with fresh supplemented medium after 1 day.

Ethics statement. The experiments involving mice were approved by the Queen's University Belfast's Ethics Committee and conducted in accordance with the UK Home Office regulations (project license PPL2778). Female C57BL/6 mice (8 to 9 weeks of age) were mock infected with phosphate-buffered saline (PBS) ($n = 4$) and infected with the wild-type strain ($n = 4$). Animals were randomized for interventions, but researchers processing the samples and analyzing the data were aware which intervention group corresponded to which cohort of animals.

Intranasal murine infection model. Female mice were infected intranasally with $\sim 3 \times 10^5$ Kp52145 in 30 μ l PBS ($n = 4$). Control mice were inoculated with 30 μ l sterile PBS ($n = 4$). After 48 h, mice were euthanized using a schedule 1 method according to UK Home Office-approved protocols. Right lung samples from infected and uninfected control mice were immersed in 1 ml of sterile PBS on ice. Samples were homogenized using a VDI 12 tissue homogenizer, and protein was quantified using a bicinchoninic acid (BCA) protein assay kit (Thermo Scientific). One hundred micrograms of total lung protein was lysed in 2 \times sample buffer (4% [wt/vol] SDS, 10% [vol/vol] 2-mercaptoethanol, 20% [wt/vol] glycerol, 0.004% [wt/vol] bromophenol blue, 0.125 M Tris-HCl [pH 6.8]), sonicated for 10 s at 10% amplitude (Branson Sonifier), boiled at 95°C for 5 min, and centrifuged at 12,000 $\times g$ for 1 min. Fifty micrograms of total lung protein was resolved by standard 8% SDS-PAGE and electroblotted onto nitrocellulose membranes for immunoblotting.

Bacterial strains. Kp52145 is a clinical isolate (serotype O1:K2) previously described (49, 57). 52145 Δwca_{k2} is an isogenic mutant of Kp52145 lacking capsule that has been previously described (58). To generate the 52145 Δglf mutant lacking the O-antigen of LPS and the 52145 $\Delta wca_{k2} \Delta glf$ mutant, a 904-bp product from the center of the *glf* gene was amplified using primers Kp52_glf_F2 (5'-GCATGA ATTCATGGTACATGTCTATGGACC-3') and Kp52_glf_R2 (5'-GCATGAATTCATCCATATCAAGGTAACGG-3') and digested with EcoRI. This was then ligated into plasmid pSF100 which had been linearized with EcoRI. The resulting plasmid pSF100-*glf* was transformed into *E. coli* β 2163, mobilized by conjugation into Kp52145 and 52145 Δwca_{k2} , and integrated into the chromosome, disrupting the *glf* gene. The resulting integrants were selected by growth on LB plates supplemented with carbenicillin at 50 μ g ml⁻¹. Chromosomal integration of the plasmid was confirmed by PCR, and loss of the O-antigen was confirmed by LPS extraction and SDS-PAGE analysis.

Infection conditions. Bacteria were grown in 5 ml LB at 37°C, harvested at exponential phase (2,500 $\times g$, 20 min), and adjusted to an optical density of 1.0 at 600 nm in PBS (5 $\times 10^8$ CFU ml⁻¹). Infections were performed using a multiplicity of infection (MOI) of 100 bacteria per cell. Infections were performed in the same medium used to maintain the cell line without antibiotics and incubated at 37°C in a humidified 5% CO₂ incubator. THP-1 monocytes were differentiated into macrophages using phorbol 12-myristate 13-acetate (PMA) at 5 ng ml⁻¹ at the time of seeding, and infections were performed 2 days later. Infections of MH-S and iBMDMs were performed the day after seeding. In all macrophage infections extending beyond 1 h, the medium was replaced after 1 h with fresh medium containing 100 μ g ml⁻¹ gentamicin (Sigma) to kill extracellular bacteria. To synchronize infections, plates were centrifuged at 200 $\times g$ for 5 min. Infections of epithelial cells (A549 and NuLi-1) were performed 2 days after seeding, with starvation for 16 h before infection using RPMI 1640 medium (Gibco 21875) supplemented only with 10 mM HEPES.

Transfection conditions. Transfection of A549 cells with siRNAs or plasmids was carried out using Lipofectamine 2000 (Invitrogen) lipofection reagent according to manufacturer's instructions. For transfection of siRNAs, 1.2 $\times 10^5$ cells (12-well plate) were transfected in suspension with 20 nM siRNA using 2 μ l of Lipofectamine 2000 in a final volume of 1 ml. Infections were carried 48 h posttransfection.

All siRNA duplexes used for *in vitro* studies were chemically synthesized by Dharmacon (GE Healthcare). The following siRNAs sense sequences were used: hSEN1 (5'-GUG AAC CAC AAC UCC GTA UUC-3' [59]), hSEN2 (5'-GGG AGU GAU UGU GGA AUG UTT-3' [59]), hSEN3 (5'-GCU UCC GAG UGG CUU AUA ATT-3' [59]), hSEN5 (5'-GUC CAC UGG UCU CUC AUU ATT-3' [59]), hSEN6 (5'-GAC UUA ACA UGU UGA GCA ATT-3' [59]), hSEN7 (5'-CAA AGU ACC GAG UCG AAU AUU-3' [59]), hCSN5 (5'-GGA UCA CCA UUA CUU UAA GTT-3' [60]), hSKP1 (5'-GGA AGA UUU GGG AAU GGA U-3'), hCUL1 (5'-UUG UGC CUA CCU CAA UAG AUU UU-3'), hRBX1 (5'-AACUGUGCAUCUGCAGGAACAA-3'), hBTRC (5'-GUG GAA UUU GUG GAA CAU

C-3'), and hSKP2 (5'-ACU CAA GUC CAG CCA UAA G-3'). An AllStars (AS) negative control scrambled siRNA (Qiagen) with no homology to any known mammalian gene was used as a negative control. Efficiency of transfection was confirmed by qPCR analysis of duplicate samples from three independent transfections by normalizing to the glyceraldehyde 3-phosphate dehydrogenase (*hGAPDH*) gene and comparing gene expression in the knockdown sample with the AllStars negative control. Primers used are listed in Table S1 in the supplemental material. The percentage of knockdown is presented in Fig. S7.

For transfection of plasmids in A549, 5×10^4 (24-well) or 1.2×10^5 (12-well) cells were seeded and, the next day, transfected with $2 \mu\text{l}$ (24-well) or $4 \mu\text{l}$ (12-well) of Lipofectamine 2000 and 1 (24-well) or $2 \mu\text{g}$ (12-well) of plasmid in a final volume of 0.5 or 1 ml, respectively.

For transfection of plasmids in MH-S, 5.0×10^5 (12-well) cells were seeded and, the next day, transfected with $4 \mu\text{l}$ of Lipofectamine 2000 and $2 \mu\text{g}$ of plasmid in a final volume of 1 ml. Experiments using plasmid-transfected cells were carried out 24 h posttransfection.

The following plasmids were used: pcDNA3 (Invitrogen), pSUMO1 (pcDNA3-HA-SUMO1 was a gift from Junying Yuan, Addgene plasmid 21154), pSENP2-GFP (pEGFP-C2 SENP2 was a gift from Mary Dasso, Addgene plasmid 13382), GSK3 β -WT (HA GSK3 beta wt pcDNA3 was a gift from Jim Woodgett, Addgene plasmid 14753), GSK3 β -S9A (HA GSK3 beta S9A pcDNA3 was a gift from Jim Woodgett, Addgene plasmid 14754). Plasmids were purified from a host *E. coli* C600 strain using an Endofree Maxi-Prep kit from Qiagen according to the manufacturer's recommendations.

Immunoblot analysis. Macrophages were seeded in 12-well plates (5.0×10^5 cells per well) and grown for 24 h. A549 cells were seeded in 12-well plates (1.2×10^5 cells per well) and grown for 48 h prior to infection. Cells were infected with *K. pneumoniae* strains for different time points as indicated in the figure legends. Cells were then washed in 1 ml of ice-cold PBS and lysed in $80 \mu\text{l}$ of $2\times$ sample buffer. The cell lysates were sonicated for 10 s at 10% amplitude (Branson Sonifier), boiled at 95°C for 5 min, and centrifuged at $12,000 \times g$ for 1 min. Twenty percent of the cell lysates were resolved by standard 8% or 12% SDS-PAGE and electroblotted onto nitrocellulose membranes. Membranes were blocked with 4% bovine serum albumin (wt/vol) in Tris-buffered saline with Tween 20 (TBST), and protein bands were detected with specific antibodies using chemiluminescence reagents and a G:BOX Chemi XRQ chemiluminescence imager (Syngene) or using fluorescent antibodies and imaging in a LI-COR Odyssey model 9120 imager.

The following antibodies were used: anti-SUMO1 antibody ($1 \mu\text{g}$, Sigma S8070), used throughout the manuscript except in Fig. 1D, 2G, 4C, and 55B, where anti-SUMO1 antibody (1:1,000, Santa Cruz Biotechnology sc-9060) was used, as indicated in the figure legends, anti-SUMO2/3 (1:1,000, Santa Cruz Biotechnology sc-32873), anti-Ubc9 (1:1,000, Santa Cruz Biotechnology sc-10759), anti-SENP2 (1:1,000, Santa Cruz Biotechnology sc-67075), anti-K48 polyubiquitin (Cell Signaling 4289), anti-cullin-1 (1:200, Santa Cruz Biotechnology sc-12761), anti-GFP (1:1,000, Cell Signaling Technologies 2955), anti-lamin A/C (1:1,000, Santa Cruz Biotechnology sc-6215), anti-SAE1 (1:1,000, Sigma-Aldrich WH0010055M1), anti-SAE2 (1:1,000, Sigma-Aldrich SAB1306998), and anti-RanGAP1 (1:1,000, Santa Cruz Biotechnology sc-28322) antibodies.

Immunoreactive bands were visualized by incubation with horseradish peroxidase-conjugated goat anti-rabbit immunoglobulins (1:5,000, Bio-Rad 170-6515) or goat anti-mouse immunoglobulins (1:5,000, Bio-Rad 170-6516).

To detect multiple proteins, membranes were reprobed after stripping previously used antibodies using a pH 2.2 glycine-HCl-SDS buffer. To ensure that equal amounts of proteins were loaded, blots were reprobed with mouse anti-human tubulin (1:3,000, Sigma T5168) or anti-vinculin (1:3,000, Sigma V4505) antibodies.

SUMO1 smears above the 90-kDa mark (excluding, therefore, the high intensity RanGAP1 bands present at 80 kDa) were quantified using Image Studio Lite version 5.2 (LI-COR) and normalized to α -tubulin. Graphs represent fold change compared to untreated noninfected cells as indicated in figure legends.

Coimmunoprecipitation analysis. Cells were seeded (3×10^5 cells per well) in six-well plates, and two wells were used per sample. At the designated time points, cells were washed with prechilled PBS (1 ml) and then lysed with $500 \mu\text{l}$ of prechilled radioimmunoprecipitation assay (RIPA) buffer (1% [wt/vol] Triton X-100, 1% [wt/vol] sodium deoxycholate, 0.1% [wt/vol] SDS, 0.15 M NaCl, 50 mM Tris-HCl [pH 7.2], 1 mM phenylmethylsulfonyl fluoride [PMSF], and Halt protease inhibitor cocktail [Thermo Scientific]) for 30 min on ice. Lysates were centrifuged at $12,000 \times g$ for 15 min at 4°C . Supernatants were transferred to prechilled tubes and incubated for 2 h with the appropriate antibody ($1 \mu\text{g}$) at 4°C with rocking. This was followed by the addition of protein A/G agarose beads ($20 \mu\text{l}$ per sample; Santa Cruz Biotechnology sc-2003) and incubation overnight at 4°C with rocking. Immunoprecipitates were collected by centrifugation at $1,000 \times g$ for 2 min at 4°C , and the beads were then washed two times with RIPA buffer ($500 \mu\text{l}$) lacking the protease inhibitor mixture. The beads were resuspended in $2\times$ sample buffer ($40 \mu\text{l}$) and boiled for 5 min at 95°C . Samples were centrifuged at $12,000 \times g$ for 1 min and subjected to immunoblotting. The immunoreactive bands were detected by incubation with Clean-Blot IP detection reagent (1:1,000, Thermo Scientific 21230).

Nuclear fractionation. A549 cells were seeded in six-well tissue culture plates at a density of 3×10^5 cells per well and infected after 2 days at an MOI of 100:1. Cells were collected in $500 \mu\text{l}$ of PBS and spun for 4 min at $1,000 \times g$ at 4°C . The pellet was resuspended in $100 \mu\text{l}$ of cytoplasmic extract buffer (10 mM HEPES, 60 mM KCl, 1 mM EDTA, 0.075% [wt/vol] Triton X-100, 1 mM PMSF, 1 mM dithiothreitol [DTT], and Halt protease inhibitor cocktail, pH 7.6) and incubated on ice for 4 min. The mixture was then spun at $1,000 \times g$ for 4 min at 4°C . The cytoplasmic extract corresponding to the supernatant fraction was mixed

with sample buffer (5×). The pellet was washed in 100 μ l of cytoplasmic buffer without Triton X-100 and resuspended in 100 μ l of sample buffer (2×).

Intracellular survival determination. MH-5 cells were seeded in 12-well plates at a density of 5×10^5 cells per well and infected the following day at an MOI of 100:1. Plates were incubated at 37°C in a humidified 5% CO₂ atmosphere. After 30 min contact, cells were washed with PBS and incubated for additional 150 min with 1 ml RPMI 1640 containing 10% FCS, 10 mM HEPES, and gentamicin (100 μ g ml⁻¹) to eliminate extracellular bacteria. To determine intracellular bacterial load, cells were washed twice with PBS and lysed with 300 μ l of 0.1% (wt/vol) saponin in PBS for 5 min at 37°C. Serial dilutions were plated on LB to quantify the number of intracellular bacteria. Bacterial adhesion was determined by serial dilutions after lysis with saponin at the time of contact (30 min), as described before. Bacterial load is represented as CFU per well. All experiments were carried out with duplicate samples on at least five independent occasions.

Microscopy. A549 cells were seeded (5×10^4 cells per well) in 24-well plates with sterile round glass coverslips and grown for 24 h to 70% to 80% confluence. Cells were transfected using Lipofectamine 2000 with plasmids encoding pEGFP-C2 SENP2 (gift from Mary Dasso, Addgene plasmid 13382) and infected 24 h later. After 5 h of incubation with either *K. pneumoniae* or PBS (control), medium was removed, and the cells were gently washed twice with PBS. Cells were then fixed by the addition of 2% (wt/vol) paraformaldehyde (250 μ l) for 20 min. Cells were washed twice with PBS and kept at 4°C in PBS supplemented with 1 mM NH₄Cl until staining. Nuclei were stained with Hoechst 33342 (1.5 μ g ml⁻¹; Sigma) for 2 h, washed with PBS and were mounted with ProLong Gold antifade mountant (Molecular Probes Inc.). Fluorescence images were captured using the $\times 40$ lens objective on a Leica DM5500 microscope equipped with the appropriate filter sets. Acquired images were analyzed using LAS imaging software (Leica).

MicroRNA analysis. Cells were washed in PBS, and miRNA was extracted using the mirPremier microRNA isolation kit (Sigma) according to the manufacturer's instructions. cDNA was generated from 100 ng of miRNA-enriched RNA using the NCode VILO miRNA cDNA synthesis kit (Invitrogen) according to the manufacturer's recommendations. Samples were assayed by quantitative real-time PCR using KAPA SYBR FAST (KAPA Biosystems) and a Stratagene Mx3005P qPCR system (Agilent Technologies). Primers were designed using the software miRprimer (61) and are listed in Table S1. Thermal cycling conditions were as follows: 50°C for 2 min for UDG incubation, 95°C for 3 min for enzyme activation, 42 cycles of denaturation at 95°C for 15 s and 1 min annealing and amplification at 60°C, followed by melt curve analysis (1 min at 95°C, 30 s at 60°C, ramping to 30 s at 95°C). Each cDNA sample was tested in duplicates, and relative mRNA quantity was determined by the comparative threshold cycle ($\Delta\Delta C_T$) method using *snoRNA-202* miRNA gene normalization.

For inhibition of the specific miRNAs in cells, 20 nM corresponding antagomir was transfected using Lipofectamine RNAiMax (Invitrogen) 24 h before infection at the time of macrophage seeding (5×10^5 cells per well). Mouse miRIDIAN microRNA hairpin inhibitors were purchased from Dharmacon: negative control (catalog number IN-001005-01-05), *mmu-let-7b-5p* (catalog number IH-310504-07-0002), *mmu-let-7f-5p* (catalog number IH-310509-08-0002), *mmu-let-7g-5p* (catalog number IH-3100374-08-0002), and *mmu-let-7i-5p* (catalog number IH-310375-08-0002). Efficiency of transfection was confirmed by quantitative PCR (qPCR) analysis of duplicate samples by comparing gene expression with the negative control. Samples were collected as described above 24 h posttransfection, from three independent transfections, and data are presented in Fig. S7.

RNA extraction and quantitative real-time PCR analysis. Cells were washed twice in PBS, and RNA was extracted using TRIzol reagent (Ambion) according to the manufacturer's instructions. Duplicate cDNA preparations from each sample were generated from 1 μ g of RNA using Moloney murine leukemia virus (M-MLV) reverse transcriptase (Sigma-Aldrich) according to the manufacturer's instructions. Quantitative real-time PCR analysis of gene expression was undertaken using the KAPA SYBR FAST qPCR kit and the Stratagene Mx3005P qPCR system (Agilent Technologies). Thermal cycling conditions were as follows: 95°C for 3 min for enzyme activation, 40 cycles of denaturation at 95°C for 10 s and annealing at 60°C for 20 s. Primers used in qPCRs are listed in Table S1. cDNA samples were tested in duplicates, and relative mRNA quantity was determined by the comparative threshold cycle ($\Delta\Delta C_T$) method, using hypoxanthine phosphoribosyltransferase 1 (*mHprt*) gene normalization for mouse samples or the glyceraldehyde 3-phosphate dehydrogenase (*hGAPDH*) gene for human samples.

Quantification of cytokines. Infections were performed in 12-well plates (1.2×10^5 cells per well for A549 and 5.0×10^5 cells per well for MH-5) using Kp52145 at an MOI of 100:1. Supernatants from infected cells were collected at the time points indicated in the figure legends and spun down at 12,000 $\times g$ for 5 min to remove any debris. TNF- α in the supernatants was determined using a Murine TNF- α standard 3,3',5,5'-tetramethylbenzidine (TMB) enzyme-linked immunosorbent assay (ELISA) development kit (PeproTech, catalog number 900-T54) and a human IL-8 standard TMB ELISA development kit (PeproTech, catalog number 900-T18), according to the manufacturer's instructions. Experiments were run in duplicates and repeated at least three times.

For quantification of type I IFN (IFN- α/β) in the supernatants of iBMDMs, cells were seeded (12-well plate, 5×10^4 cells per well) and grown for 24 h. Cells were then infected (MOI, 100:1) for 3 h, and supernatants were collected. Murine type I IFNs were detected using B16-Blue IFN- α/β reporter cells (Invivogen) which carry an SEAP reporter gene under the control of the IFN- α/β -inducible ISG54 promoter and that have an inactivation of the IFN- γ receptor. Briefly, supernatants from iBMDM infections were incubated with the reporter cell line, and levels of SEAP in the supernatants were determined using the detection medium QUANTI-Blue (Invivogen) after 24 h as per the manufacturer's instructions using recombinant mouse IFN- β (PBL Assay Science, catalog number 12401-1) as a standard.

Statistical analysis. Statistical analyses were performed using analysis of variance (ANOVA) or, when the requirements were not met, by unpaired *t* test. Multiple comparison was performed using Holm-Sidak's multiple-comparison test. *P* values of <0.05 were considered statistically significant. Normality and equal variance assumptions were tested with the Kolmogorov-Smirnov test and the Brown-Forsythe test, respectively. All analyses were performed using GraphPad Prism for Windows (version 5.03) software.

SUPPLEMENTAL MATERIAL

Supplemental material is available online only.

FIG S1, TIF file, 0.5 MB.

FIG S2, TIF file, 1.4 MB.

FIG S3, TIF file, 0.6 MB.

FIG S4, TIF file, 0.5 MB.

FIG S5, TIF file, 0.8 MB.

FIG S6, TIF file, 0.2 MB.

FIG S7, TIF file, 0.1 MB.

TABLE S1, DOCX file, 0.1 MB.

ACKNOWLEDGMENTS

We thank the members of the J.A.B. laboratory for their thoughtful discussions and support with this project. We thank Daniel Longley for kindly providing us with the SCF siRNAs for Skp1, Cul-1, RBX1, Skp2, and β TrCP used in this study.

L.H. is a recipient of the Queen's University Belfast Research Fellowship. K.P. and F.N.V. are fellows funded by European Union Seventh Framework Program Marie Curie Initial Training Networks (FP7-PEOPLE-2012-ITN) for the project INBIONET under grant agreement PITN-GA-2012-316682. This work was supported by a Marie Curie Career Integration Grant U-KARE (PCIG13-GA-2013-618162), the Biotechnology and Biological Sciences Research Council (BBSRC, BB/L007223/1 and BB/P006078/1), and Queen's University Belfast start-up funds to J.A.B.

J.S.-P. and J.A.B. conceived the study and wrote the first draft of the manuscript. J.S.-P., K.P., F.N.V., A.D., C.G.F., and L.H. performed the experiments and contributed data for this work. J.S.-P., K.P., F.N.V., A.D., C.G.F., L.H., and J.A.B. contributed to and approved the final version of the manuscript.

We declare no conflict of interest.

REFERENCES

- Hendriks IA, Vertegaal ACO. 2016. A comprehensive compilation of SUMO proteomics. *Nat Rev Mol Cell Biol* 17:581–595. <https://doi.org/10.1038/nrm.2016.81>.
- Flotho A, Melchior F. 2013. Sumoylation: a regulatory protein modification in health and disease. *Annu Rev Biochem* 82:357–385. <https://doi.org/10.1146/annurev-biochem-061909-093311>.
- Shin EJ, Shin HM, Nam E, Kim WS, Kim JH, Oh BH, Yun Y. 2012. DeSUMOylating isopeptidase: a second class of SUMO protease. *EMBO Rep* 13:339–346. <https://doi.org/10.1038/embor.2012.3>.
- Everett RD, Boutell C, Hale BG. 2013. Interplay between viruses and host sumoylation pathways. *Nat Rev Microbiol* 11:400–411. <https://doi.org/10.1038/nrmicro3015>.
- Ribet D, Hamon M, Gouin E, Nahori M, Impens F, Neyret-Kahn H, Gevaert K, Vandekerckhove J, Dejean A, Cossart P. 2010. *Listeria monocytogenes* impairs SUMOylation for efficient infection. *Nature* 464:1192–1195. <https://doi.org/10.1038/nature08963>.
- Verma S, Mohapatra G, Ahmad SM, Rana S, Jain S, Khalsa JK, Srikanth CV. 2015. *Salmonella* engages host microRNAs to modulate SUMOylation: a new arsenal for intracellular survival. *Mol Cell Biol* 35:2932–2946. <https://doi.org/10.1128/MCB.00397-15>.
- Sidik SM, Salsman J, Dellaire G, Rohde JR. 2015. *Shigella* infection interferes with SUMOylation and increases PML-NB number. *PLoS One* 10:e0122585. <https://doi.org/10.1371/journal.pone.0122585>.
- Lapaquette P, Fritah S, Lhocine N, Andrieux A, Nigro G, Mounier J, Sansonetti P, Dejean A. 2017. *Shigella* entry unveils a calcium/calpain-dependent mechanism for inhibiting sumoylation. *Elife* 6:e27444. <https://doi.org/10.7554/eLife.27444>.
- Paczosa MK, Mecsas J. 2016. *Klebsiella pneumoniae*: going on the offense with a strong defense. *Microbiol Mol Biol Rev* 80:629–661. <https://doi.org/10.1128/MMBR.00078-15>.
- Wieland CW, Van Lieshout MHP, Hoogendijk AJ, Van Der Poll T. 2011. Host defence during *Klebsiella pneumoniae* relies on haematopoietic-expressed Toll-like receptors 4 and 2. *Eur Respir J* 37:848–857. <https://doi.org/10.1183/09031936.00076510>.
- Branger J, Knapp S, Weijer S, Leemans JC, Pater JM, Speelman P, Florquin S, van der Poll T. 2004. Role of Toll-like receptor 4 in Gram-positive and Gram-negative pneumonia in mice. *Infect Immun* 72:788–794. <https://doi.org/10.1128/iai.72.2.788-794.2004>.
- Tomás A, Lery L, Regueiro V, Pérez-Gutiérrez C, Martínez V, Moranta D, Llobet E, González-Nicolau M, Insua JL, Tomas JM, Sansonetti PJ, Tournebise R, Bengoechea JA. 2015. Functional genomic screen identifies *Klebsiella pneumoniae* factors implicated in blocking nuclear factor κ B (NF- κ B) signaling. *J Biol Chem* 290:16678–16697. <https://doi.org/10.1074/jbc.M114.621292>.
- Regueiro VVV, Moranta D, Campos MA, Margareto J, Garmendia J, Bengoechea J. 2009. *Klebsiella pneumoniae* increases the levels of Toll-like receptors 2 and 4 in human airway epithelial cells. *Infect Immun* 77:714–724. <https://doi.org/10.1128/IAI.00852-08>.
- Frank CG, Regueiro V, Rother M, Moranta D, Maeurer AP, Garmendia J, Meyer TF, Bengoechea JA. 2013. *Klebsiella pneumoniae* targets an EGF receptor-dependent pathway to subvert inflammation. *Cell Microbiol* 15:1212–1233. <https://doi.org/10.1111/cmi.12110>.
- Regueiro VVV, Moranta D, Frank CG, Larrarte E, Margareto J, March C, Garmendia J, Bengoechea J. 2011. *Klebsiella pneumoniae* subverts the

- activation of inflammatory responses in a NOD1-dependent manner. *Cell Microbiol* 13:135–153. <https://doi.org/10.1111/j.1462-5822.2010.01526.x>.
16. Lery LMS, Frangeul L, Tomas A, Passet V, Almeida AS, Bialek-Davenet S, Barbe V, Bengoechea JA, Sansonetti P, Brisse S, Tournebise R. 2014. Comparative analysis of *Klebsiella pneumoniae* genomes identifies a phospholipase D family protein as a novel virulence factor. *BMC Biol* 12:41. <https://doi.org/10.1186/1741-7007-12-41>.
 17. Regueiro V, Campos MA, Pons J, Albertí S, Bengoechea JA. 2006. The uptake of a *Klebsiella pneumoniae* capsule polysaccharide mutant triggers an inflammatory response by human airway epithelial cells. *Microbiology (Reading)* 152:555–566. <https://doi.org/10.1099/mic.0.28285-0>.
 18. Nayak A, Müller S. 2014. SUMO-specific proteases/isopeptidases: SENPs and beyond. *Genome Biol* 15:422. <https://doi.org/10.1186/s13059-014-0422-2>.
 19. Hang J, Dasso M. 2002. Association of the human SUMO-1 protease SENP2 with the nuclear pore. *J Biol Chem* 277:19961–19966. <https://doi.org/10.1074/jbc.M201799200>.
 20. Itahana Y, Yeh ETH, Zhang Y. 2006. Nucleocytoplasmic shuttling modulates activity and ubiquitination-dependent turnover of SUMO-specific protease 2. *Mol Cell Biol* 26:4675–4689. <https://doi.org/10.1128/MCB.01830-05>.
 21. Willems AR, Schwab M, Tyers M. 2004. A hitchhiker's guide to the cullin ubiquitin ligases: SCF and its kin. *Biochim Biophys Acta* 1695:133–170. <https://doi.org/10.1016/j.bbamcr.2004.09.027>.
 22. Collier-Hyams LS, Sloane V, Batten BC, Neish AS. 2005. Cutting edge: bacterial modulation of epithelial signaling via changes in neddylation of cullin-1. *J Immunol* 175:4194–4198. <https://doi.org/10.4049/jimmunol.175.7.4194>.
 23. Kumar A, Wu H, Collier-Hyams LS, Hansen JM, Li T, Yamoah K, Pan Z-Q, Jones DP, Neish AS. 2007. Commensal bacteria modulate cullin-dependent signaling via generation of reactive oxygen species. *EMBO J* 26:4457–4466. <https://doi.org/10.1038/sj.emboj.7601867>.
 24. Wu J, Lin H, Hu Y, Chien C. 2005. Neddylation and deneddylation regulate Cul1 and Cul3 protein accumulation. *Nat Cell Biol* 7:1014–1020. <https://doi.org/10.1038/ncb1301>.
 25. Wang J, Barnes RO, West NR, Olson M, Chu JE, Watson PH. 2008. Jab1 is a target of EGFR signaling in ERalpha-negative breast cancer. *Breast Cancer Res* 10:R51. <https://doi.org/10.1186/bcr2105>.
 26. At L, Floor QS, Broug-Holub E, Toews GB, Iwaarden J, Strieter RM, Kunkel SL, Iii RP, Standiford TJ, van Iwaarden JF. 1997. Alveolar macrophages are required for protective pulmonary defenses in murine *Klebsiella pneumoniae*: elimination of alveolar macrophages increases neutrophil recruitment but decreases bacterial clearance and survival. *Infect Immun* 65:1139–1146. <https://doi.org/10.1128/IAI.65.4.1139-1146.1997>.
 27. Xiong H, Keith JWW, Samilo DWW, Carter RAA, Leiner IMM, Pamer EGG. 2016. Innate lymphocyte/Ly6Chi monocyte crosstalk promotes *Klebsiella pneumoniae* clearance. *Cell* 165:679–689. <https://doi.org/10.1016/j.cell.2016.03.017>.
 28. March C, Cano V, Moranta D, Llobet E, Pérez-Gutiérrez C, Tomás JM, Suárez T, Garmendia J, Bengoechea JA. 2013. Role of bacterial surface structures on the interaction of *Klebsiella pneumoniae* with phagocytes. *PLoS One* 8:e56847. <https://doi.org/10.1371/journal.pone.0056847>.
 29. Yang F-L, Yang Y-L, Liao P-C, Chou J-C, Tsai K-C, Yang A-S, Sheu F, Lin T-L, Hsieh P-F, Wang J-T, Hua K-F, Wu S-H. 2011. Structure and immunological characterization of the capsular polysaccharide of a pyrogenic liver abscess caused by *Klebsiella pneumoniae*: activation of macrophages through toll-like receptor 4. *J Biol Chem* 286:21041–21051. <https://doi.org/10.1074/jbc.M1111.222091>.
 30. Takeuchi O, Akira S. 2010. Pattern recognition receptors and inflammation. *Cell* 140:805–820. <https://doi.org/10.1016/j.cell.2010.01.022>.
 31. Boxx GM, Cheng G. 2016. The roles of type I interferon in bacterial infection. *Cell Host Microbe* 19:760–769. <https://doi.org/10.1016/j.chom.2016.05.016>.
 32. Ivin M, Dumigan A, de Vasconcelos FN, Ebner F, Borroni M, Kavirayani A, Przybyszewska KN, Ingram RJ, Lienenklaus S, Kalinke U, Stoiber D, Bengoechea JA, Kovarik P. 2017. Natural killer cell-intrinsic type I IFN signaling controls *Klebsiella pneumoniae* growth during lung infection. *PLoS Pathog* 13:e1006696. <https://doi.org/10.1371/journal.ppat.1006696>.
 33. Ohno M, Natsume A, Kondo Y, Iwamizu H, Motomura K, Toda H, Ito M, Kato T, Wakabayashi T. 2009. The modulation of microRNAs by type I IFN through the activation of signal transducers and activators of transcription 3 in human glioma. *Mol Cancer Res* 7:2022–2030. <https://doi.org/10.1158/1541-7786.MCR-09-0319>.
 34. Sahin U, Ferhi O, Carnec X, Zamborlini A, Peres L, Jollivet F, Vitaliano-Prunier A, de The H, Lallemand-Breitenbach V. 2014. Interferon controls SUMO availability via the Lin28 and let-7 axis to impede virus replication. *Nat Commun* 5:4187. <https://doi.org/10.1038/ncomms5187>.
 35. Li X, Zhou X, Ye Y, Li Y, Li J, Privratsky B, Wu E, Gao H, Huang C, Wu M. 2014. Lyn regulates inflammatory responses in *Klebsiella pneumoniae* infection via the p38/NF- κ B pathway. *Eur J Immunol* 44:763–773. <https://doi.org/10.1002/eji.201343972>.
 36. Ahn D, Peñaloza H, Wang Z, Wickersham M, Parker D, Patel P, Koller A, Chen EI, Bueno SM, Uhlemann A-C, Prince A. 2016. Acquired resistance to innate immune clearance promotes *Klebsiella pneumoniae* ST258 pulmonary infection. *JCI Insight* 1:e89704. <https://doi.org/10.1172/jci.insight.89704>.
 37. Cano V, March C, Insua JL, Aguiló N, Llobet E, Moranta D, Regueiro V, Brennan GP, Millán-Lou MI, Martín C, Garmendia J, Bengoechea JA. 2015. *Klebsiella pneumoniae* survives within macrophages by avoiding delivery to lysosomes. *Cell Microbiol* 17:1537–1560. <https://doi.org/10.1111/cmi.12466>.
 38. Kim J-G, Stork W, Mudgett MB. 2013. Xanthomonas type III effector XopD desumoylates tomato transcription factor SIERF4 to suppress ethylene responses and promote pathogen growth. *Cell Host Microbe* 13:143–154. <https://doi.org/10.1016/j.chom.2013.01.006>.
 39. Orth K, Xu Z, Mudgett MB, Bao ZQ, Palmer LE, Bliska JB, Mangel WF, Staskawicz B, Dixon JE. 2000. Disruption of signaling by yersinia effector YopJ, a ubiquitin-like protein protease. *Science* 290:1594–1597. <https://doi.org/10.1126/science.290.5496.1594>.
 40. Petroski MD, Deshaies RJ. 2005. Function and regulation of cullin-RING ubiquitin ligases. *Nat Rev Mol Cell Biol* 6:9–20. <https://doi.org/10.1038/nrm1547>.
 41. Jones J, Wu K, Yang Y, Guerrero C, Nillegoda N, Pan Z-Q, Huang L. 2008. A targeted proteomic analysis of the ubiquitin-like modifier Nedd8 and associated proteins. *J Proteome Res* 7:1274–1287. <https://doi.org/10.1021/pr700749v>.
 42. Liu YS, Shepherd EG, Nelin LD. 2007. MAPK phosphatases - regulating the immune response. *Nat Rev Immunol* 7:202–212. <https://doi.org/10.1038/nri2035>.
 43. Sun S-C. 2008. Deubiquitylation and regulation of the immune response. *Nat Rev Immunol* 8:501–511. <https://doi.org/10.1038/nri2337>.
 44. Decque A, Joffre O, Magalhaes JG, Cossec J-C, Blecher-Gonen R, Lapaquette P, Silvain A, Manel N, Joubert P-E, Seeler J-S, Albert ML, Amit I, Amigorena S, Dejean A. 2016. Sumoylation coordinates the repression of inflammatory and anti-viral gene-expression programs during innate sensing. *Nat Immunol* 17:140–149. <https://doi.org/10.1038/ni.3342>.
 45. González-Navajas JM, Lee J, David M, Raz E. 2012. Immunomodulatory functions of type I interferons. *Nat Rev Immunol* 12:125–135. <https://doi.org/10.1038/nri3133>.
 46. Callegari S, Gastaldello S, Faridani OR, Masucci MG. 2014. Epstein-Barr virus encoded microRNAs target SUMO-regulated cellular functions. *FEBS J* 281:4935–4950. <https://doi.org/10.1111/febs.13040>.
 47. Staedel C, Darfeuille F. 2013. MicroRNAs and bacterial infection. *Cell Microbiol* 15:1496–1507. <https://doi.org/10.1111/cmi.12159>.
 48. Chen X-M, Splinter PL, O'Hara SP, LaRusso NF. 2007. A cellular micro-RNA, let-7i, regulates Toll-like receptor 4 expression and contributes to cholangiocyte immune responses against *Cryptosporidium parvum* infection. *J Biol Chem* 282:28929–28938. <https://doi.org/10.1074/jbc.M702633200>.
 49. Cortés G, Borrell N, De Astorza B, Gómez C, Sauleda J, Albertí S. 2002. Molecular analysis of the contribution of the capsular polysaccharide and the lipopolysaccharide O side chain to the virulence of *Klebsiella pneumoniae* in a murine model of pneumonia. *Infect Immun* 70:2583–2590. <https://doi.org/10.1128/iai.70.5.2583-2590.2002>.
 50. Lawlor MS, Hsu J, Rick PD, Miller VL. 2005. Identification of *Klebsiella pneumoniae* virulence determinants using an intranasal infection model. *Mol Microbiol* 58:1054–1073. <https://doi.org/10.1111/j.1365-2958.2005.04918.x>.
 51. Fritah S, Lhocine N, Golebiowski F, Mounier J, Andrieux A, Jouvion G, Hay RT, Sansonetti P, Dejean A. 2014. Sumoylation controls host anti-bacterial response to the gut invasive pathogen *Shigella flexneri*. *EMBO Rep* 15:965–972. <https://doi.org/10.15252/embr.201338386>.
 52. Akira S, Uematsu S, Takeuchi O. 2006. Pathogen recognition and innate immunity. *Cell* 124:783–801. <https://doi.org/10.1016/j.cell.2006.02.015>.
 53. Arpaia N, Godec J, Lau L, Sivick KE, McLaughlin LM, Jones MB, Dracheva T, Peterson SN, Monack DM, Barton GM. 2011. TLR signaling is required for *Salmonella* Typhimurium virulence. *Cell* 144:675–688. <https://doi.org/10.1016/j.cell.2011.01.031>.
 54. Bossis G, Sarry J-E, Kifagi C, Ristic M, Saland E, Vergez F, Salem T, Boutzen

- H, Baik H, Brockly F, Pelegrin M, Kaoma T, Vallar L, Récher C, Manenti S, Piechaczyk M. 2014. The ROS/SUMO axis contributes to the response of acute myeloid leukemia cells to chemotherapeutic drugs. *Cell Rep* 7:1815–1823. <https://doi.org/10.1016/j.celrep.2014.05.016>.
55. Tilemann L, Lee A, Ishikawa K, Agüero J, Rapti K, Santos-Gallego C, Kohlbrenner E, Fish KM, Kho C, Hajjar RJ. 2013. SUMO-1 gene transfer improves cardiac function in a large-animal model of heart failure. *Sci Transl Med* 5:211ra159. <https://doi.org/10.1126/scitranslmed.3006487>.
56. Kho C, Lee A, Jeong D, Oh JG, Chaanine AH, Kizana E, Park WJ, Hajjar RJ. 2011. SUMO1-dependent modulation of SERCA2a in heart failure. *Nature* 477:601–605. <https://doi.org/10.1038/nature10407>.
57. Nassif X, Sansonetti PJ. 1986. Correlation of the virulence of *Klebsiella pneumoniae* K1 and K2 with the presence of a plasmid encoding aerobactin. *Infect Immun* 54:603–608. <https://doi.org/10.1128/IAI.54.3.603-608.1986>.
58. Llobet E, Tomás JM, Bengoechea JA. 2008. Capsule polysaccharide is a bacterial decoy for antimicrobial peptides. *Microbiology (Reading)* 154:3877–3886. <https://doi.org/10.1099/mic.0.2008/022301-0>.
59. Liu X, Chen W, Wang Q, Li L, Wang C. 2013. Negative regulation of TLR inflammatory signaling by the SUMO-deconjugating enzyme SENP6. *PLoS Pathog* 9:e1003480. <https://doi.org/10.1371/journal.ppat.1003480>.
60. Lee Y-H, Judge AD, Seo D, Kitade M, Gómez-Quiroz LE, Ishikawa T, Andersen JB, Kim B-K, Marquardt JU, Raggi C, Avital I, Conner EA, MacLachlan I, Factor VM, Thorgeirsson SS. 2011. Molecular targeting of CSN5 in human hepatocellular carcinoma: a mechanism of therapeutic response. *Oncogene* 30:4175–4184. <https://doi.org/10.1038/onc.2011.126>.
61. Busk PK. 2014. A tool for design of primers for microRNA-specific quantitative RT-qPCR. *BMC Bioinformatics* 15:29. <https://doi.org/10.1186/1471-2105-15-29>.